Renewable Energy 227 (2024) 120398

Contents lists available at ScienceDirect

Renewable Energy

journal homepage: www.elsevier.com/locate/renene

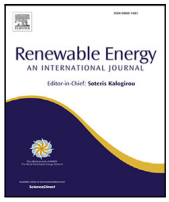

Parametric energy optimization of a ventilated facade with windows in Mediterranean climates

Carlos-Antonio Domínguez-Torres [a,*], Rafael Suárez [b], Angel Luis León-Rodríguez [b], Antonio Domínguez-Delgado [c]

[a] Escuela Técnica Superior de Arquitectura, Universidad de Sevilla, Avda.Reina Mercedes 2, 41012, Sevilla, Spain
[b] Instituto Universitario de Arquitectura y Ciencias de la Construcción, Escuela Técnica Superior de Arquitectura, Universidad de Sevilla, Avda.Reina Mercedes 2, 41012, Sevilla, Spain
[c] Department of Applied Mathematics 1, Universidad de Sevilla, Avda.Reina Mercedes 2, 41012, Sevilla, Spain

ARTICLE INFO

Keywords:
Building energy retrofit
Social housing
Parametric energy optimization
Energy savings
Three-dimensional CFD modeling

ABSTRACT

Ventilated facades are an effective passive measure to improve the energy performance of buildings in warm and temperate climates such as the Mediterranean. However, although in the Mediterranean sociocultural context the use of windows is widespread, there is a lack of energy analysis of ventilated facades in combination with windows. This is due to the lack of accurate simulation tools to evaluate the energy performance of this combination because of its complex thermodynamics, which, among other issues, requires three-dimensional computational fluid dynamic tools. In this work, a parametric energy analysis of the design parameters of a ventilated façade with window openings has been performed using a three-dimensional numerical model developed by the authors that combines turbulent Navier–Stokes thermodynamic equations for air with a set of differential equations for the envelope temperatures. The results of the analysis showed the potential of the opaque ventilated façade (OVF) with windows when applied to the rehabilitation of energetically obsolete facades, achieving a remarkable reduction in heat flux with respect to these facades, a reduction that reaches 32% for the yearly heat flux when using the optimal configuration found.

1. Introduction

In Europe, the building sector is responsible for about half of energy consumption, mainly due to the need for indoor comfort, while, at the same time, this need for indoor comfort is leading to a sharp and progressive increase in energy consumption worldwide [1]. This is the reason why regulations have been established for reducing the amount of energy consumed in buildings according to the H2030 guidelines set by the EU [2].

In relation to this issue, it is noteworthy that the energy efficiency of a large part of the European building stock is low, [3,4], mainly in older buildings that were built prior to the promulgation of the first energy regulations [5]. Because of this fact, European institutions have promoted the energy retrofitting of buildings since 2002, when the first European directive concerning the energy efficiency in buildings was released [6].

In this framework, in regions with warm climates, such as Mediterranean regions, characterized by high levels of solar irradiation and temperatures, especially in the hot season, one of the most widely used constructive solutions for retrofitting buildings is the opaque ventilated façade, which has shown its potential to reduce heat flux between outdoor and indoor spaces in the hot season and, in this way, to decrease the energy demand for cooling in the aforementioned geographical area [7–12].

On the other hand, in the geographical Mediterranean area, windows are appreciated as elements that provide aesthetic value, natural lighting, and ventilation; therefore, on many occasions in the retrofitting of façades, it may be desirable to preserve the existing windows, which is applicable to the case of retrofitting using ventilated facades.

As stated in [13], the thermal performance of the OVF is influenced by environmental parameters (mainly weather conditions), and by the OVF design parameters (geometry, materials, etc.). However, while the outer parameters cannot normally be changed, design parameters can be chosen in order to optimize the thermal performance of the OVF and specifically of the OVF used in combination with windows.

Most studies on the impact of environmental and design parameters on the energy performance of OVFs, both those carried out through numerical analyses and through monitoring campaigns, focus on the

* Corresponding author.
E-mail address: cdtorres@us.es (C.-A. Domínguez-Torres).

https://doi.org/10.1016/j.renene.2024.120398
Received 19 August 2023; Received in revised form 20 November 2023; Accepted 27 March 2024
Available online 2 April 2024

OVFs without window openings, as evidenced in the literature compilations published in [13–15]. The studies cited in these last papers deal, among other issues, with the analysis of the impact on the thermodynamic and energy performance of the OVF of some design parameters. Next, we provide a briefly description of these studies ordered by the design parameters investigated:

- Ventilation grills aperture: some works investigate the impact of considering the grill aperture opened or closed as [8], where a comparative analysis is made between a ventilated façade with open air duct and one with closed air duct or [10,11,16,17] where the OVF with ventilation opened aperture are compared to sealed cavity, concluding in all these works that in summer the opened case results in a better energy performance of the OVF to reduce thermal transfer than the closed opening aperture case, although in winter the sealed cavity performs better than the open grill [11]; however, the only work that offers results for the whole year [17] concludes an energy saving for the whole year of 9% for a South orientation and negative saving of −4% for an North orientation for the city of Madrid (Spain). Likewise, based on experimental data, in [18] the role of the grills aperture was investigated and it was concluded that the fully open grills yields greater daily thermal energy reductions than grills partially opened by comparison with the ventilation completely closed and, in [15], three grills opening ratio of 61%, 33% and 100% were investigated and, using the same metrics than in [18], it was drawn up a direct correlation between the energy yield in the warm season and the grills opening ratio, concluding that the higher the aperture ratio, the greater the potential for thermal energy decrease.
- Air channel thickness: the air channel thickness is a characteristic of the OVF that affects its energy performance being possible to find a large number of works focused in the study of this parameter [13,19]. The most common conclusion in the literature is that narrower cavities have worse energy performance [8,10,18] in order to reduce cooling loads in the hot season. Thus, in [8] is demonstrated that the energy savings increase as the air duct thickness d increases and that this energy saving increase is particularly marked by air duct thickness values lower than 0.15 m, tending for values greater than 0.15 m to a much less marked growth and some authors point out that ventilation rates decrease for thicknesses greater than 0.30 m [7,8]. Similar results are obtained in [20] for a double-skin facade; in this work it is concluded that a channel dimension that is too narrow can severely impede ventilation, while oversizing it produces only a moderately worse result than the optimal value proposed for channel width.
  However, the increase in d is related to an increase in heating loads in winter due to the rise of the air flux rate inside the ventilated cavity with a consequent increase in heat loss when the ambient temperature is cold, as is the case in winter [7,11]. Thus, changes in air channel thickness produce in summer and winter an opposite effect on the heat flux through the OVF that justifies the need for an annual calculation of the effect on such flux of any change in air channel thickness.
- Surface solar absorptivity: the surface temperature of the cladding is highly influenced by solar irradiance [21], which has implications on the temperature of the air inside the channel, on its velocity, and on the temperature of the surface of the interior wall, all of which affect the energy performance of the OVF, being necessary to analyze the effect of the changes on the solar absorptivity of the outer surface in the yearly heat flux through the OVF.
  Previous research, as developed in [18], based on experimentation in the summer season, has shown that dark colors of the outer surface of the outer layer of the OVF increase the temperature of the external skin, which produces an increased air flow rate inside the ventilated channel, as well as an increase in the radiative thermal exchange between the inner surfaces of the cavity that results in an increase in the heat flux through the OVF; the authors conclude that exterior surfaces with a lower solar absorption coefficient are more effective in reducing the heat flux through the OVF.
  Likewise, other research on the effect of the solar absorptivity of the external surface on the energy performance of ventilated façades, as developed in [8,9,15], also found that the darker the color of the exterior surface, the lower the ability of the facade to reduce heat transfer through the OVF in the hot season.
  However, according to the effect of colors on absorption of solar radiation, a positive effect can be expected in winter in order to reduce the heating loads for dark colors or, equivalently, for surfaces with a high value of solar absorptivity.
- Thermal diffusivity of the outer sheet: the thermal diffusivity of the outer sheet determines the transmission of heat through this sheet and therefore plays a determining role in the thermodynamics of the ventilated façade and, consequently, in the heat transfer through it. Previous research has shown that the energy performance of ventilated façades is most efficient for low values of the thermal diffusivity of the outer sheet as it was concluded by using simulations and mathematical solvers in [8,9] or experimental results in [18,22] under summer weather conditions.
- Insulation thickness: thermal insulation is a simple and cost-effective measure to reduce the heat flux through the envelope of buildings. Although a priori, the thicker the insulation layer, the lower the heat flux through the façade, some studies, as those performed in [23], stated that increasing the insulation thickness is only cost-effective up to a certain limit, which is in accordance with the notion of critical insulation thickness [24]. However, in the previous literature, to the best of our knowledge, there are no studies focused on the impact of changes in this parameter on the energy performance of the OVF, only in [8] is investigated how to optimize the layout of the insulating material inside the ventilated chamber, finding that energy savings are maximum for a fraction between 0.15 and 0.30 of the insulating material placed on the surface of the outer skin facing the air duct, and the authors of that work stated that the usual placement of the insulation material on the inner wall of the OVF is more effective than on the outer layer.
- Ventilated channel height: the height of the ventilated façade and therefore the height of the ventilated chamber of the OVF is another characteristic that can impact the energy performance of the façade. The most common assertion about the influence of the ventilated channel height on the thermal behavior of the OVF is that the higher the height, the higher the air velocity inside the channel, which in turn influences the heat flux through the OVF. In [9,11], based on simulation models, an increase of the air temperature inside the air chamber was found as the height increased, a result that was observed also in [25,26] based on experimental and simulation data. Similarly, different heights of OVFs have been experimentally studied in [15,22,27]; in [27], the energy performance of two 6 and 12 m high OVFs was studied in summer; it was found that during the hours of sunlight, the temperature is always higher for the 12 m façade and during the night the temperature is always lower; in [22] the energy performance of three OVFs of 4, 8 and 12 m height was studied in summer; from experimental data it was concluded that the energy performance of the lower facades is more affected by the radiation reflected from the ground than higher façades that can result in a lower efficiency in cooling for the lower façades for high values of ground solar reflectivity; in [15], three OVFs of 2.20, 3.35 and 4.40 m height were studied and the results of daily thermal

energy reductions obtained from the experimentation yield values equal to 44.1%, 45.3%, and 46.5%, and therefore support the assertion that the higher the façade, the higher the daily thermal energy reductions. Finally, in the same regard, it can be noted that in [28] an increase in air temperatures was found in the middle and upper zones of the ventilated channel, depending on where the maximum value of these temperatures is reached from the vertical shear plane inside the channel.

In light of this review, two facts can be highlighted that show a gap in the literature on ventilated facades: firstly, the absence of studies on the impact of changes in design parameters on the energy performance of an OVF equipped with window openings and, secondly, the scarce number of works that evaluate the effect of design parameter changes in the energy behavior of the OVF for all seasons of the year, which even for some of the design parameters is non-existent, making it difficult to ensure the suitability of these changes to produce year-round energy savings due to the opposite effect that changes in design parameters can have on the energy performance of the OVF in different seasons of the year.

The lack of studies on OVF with window openings is of special relevance because the windows represent a physical interruption of the air chamber and, therefore, an obstacle to the movement of air along it; this implies a genuine three-dimensional behavior of the air flux as shown in [26] and that cannot be simulated by 2D numerical models as was demonstrated in this last paper. Thus, in terms of OVFs with windows opening, its parametric optimization must be performed using three-dimensional numerical models capable of adequately simulating such facade systems and that, as stated in [29], have been validated by extensive monitoring campaigns.

In the very large literature on OVFs, to the best of our knowledge, the authors do not have found any reference analyzing the energy optimization of OVFs with window openings and then it is possible to state the existence of a gap in the literature caused by the lack of energy optimization analysis for OVFs with window openings, which is the objective of this research.

On the other hand, energy analysis needs to be extended to all seasons of the year since changes in the design parameters that can lead to savings in summer can nevertheless increase loads in winter, so it is necessary to calculate the energy whole yearly balance produced by the changes in the parameters to be able to really establish the existence or not of energy savings considering all the seasons of the year.

This paper reports a parametric analysis of the impact of changes in its design parameters on the yearly heat flux through an OVF with window openings. The analysis of this impact for changes in the façade design parameters was performed through the use of a well-validated 3D numerical model introduced in [26] where an extensive monitoring campaign was carried out and used to validate the numerical model, campaign that spanned the following time intervals: from 29 December 2020 to 5 January 2021, from 11 January to 18 January 2021, from 30 March to 13 April 2021, from 20 to 28 June 2021, and from 5 to 18 July 2021.

The energy analysis carried out allowed to find out the values of the façade design features that produce the best energy performance of the analyzed OVF, evaluated in terms of the annual heat flux through the facade and its reduction compared to an existing obsolete energy facade commonly used in housing construction in Spain in the 1960s and 1970s, before the enactment of the first legislation for energy demand of buildings in Spain, the NBE-CT-79 [30].

The results reported in this paper allow:

– to select the best option of the geometric and thermophysical parameters of the OVF in order to optimize its energy performance, providing guidelines for the design of OVFs with windows opening;

– to quantify the heat flux decrease for each studied OVF design compared to a reference case given by an obsolete energy façade allowing to retrofit this last façade by using an OVF under the criterium of best contribution in reducing the heat flux through the façade.

The paper is organized as follows: in Section 2 the methods used for the computation of the heat flux through the OVF are described; in Section 3 the methodology used in the energy optimization analysis is presented; in Section 4, the results from the optimization parametric analysis are presented and discussed; finally, in Section 5 the conclusions and future work are shown.

2. Methods

2.1. Façade description

The OVF subject of this study is the result of adding an opaque ventilated facade system to a façade with windows that reproduces the most usual constructive configuration of the façades of social housing built in the middle of the last century in large areas of southern Europe with a Mediterranean climate. These dwellings are characterized by their lack of energy insulation measures in such a way that they can be considered as very poorly adapted to the goal of energy savings consumption to achieve indoor thermal comfort.

Two full-scale outdoor test cells with configurable south-facing facades were used to carry out the present investigation. These test cells are placed at the center of Seville city (Spain) in an open-air space of the University of Seville.

The facility to which the test cells belong is configured in two separated modules. Each module consists of two test cells, one facing north and the other south, connected by a service space, Figs. 1(a) and 1(b). The inner dimensions of the cells are 3.20 m deep, 2.70 m high and 2.40 m wide.

The use of test cells to analyze the energy and thermodynamic performance of ventilated facades has been widely reported in previous scientific literature, being very common the use of full-scale test cells of the so-called PASLINK type [31,32], in which the test cells used in this paper can be framed. For example, to cite a few works, in [33] the thermal performance of a ventilated wall, both for heating and cooling, was investigated; the experimental data were obtained using a PASLINK test tell with a 2.75×2.75 m^2 removable south wall. In [34], the thermal performance of a new type of ventilated facade including a phase change material (PCM) in its outer layer was experimentally analyzed using a full-scale PASLINK test cell installation equipped with a 2.7×2.7 m^2 prototype facade. In [35], a ventilated façade is analyzed using the Paslink cell-based test methodology to perform the experimental test. In [36] three Passlink-inspired test cells were used to explore three constructive systems, including an OVF, for the retrofitting of energy-obsolete facades. In [37] a full-size test cell is used to compare the thermophysical behavior of three opaque ventilated facades, characterized by different positions of the mass (hollow bricks) inside the air space, and in [26] a test cell, like the one used in the present work, is used to experimentally study the energy performance of an OVF installed on a façade equipped with a window.

In short, a fairly large number of works, of which only a brief sample has been referred to, use test cells of similar or comparable dimensions to those used in this work in order to analyze the energy performance of ventilated facades.

The test cell named as Cell 3 in Fig. 1(a) reproduces in its southern customizable wall a facade with poor thermal insulation commonly built in social housing in southern Spain in the middle decades of the twentieth century. The transmittance of this wall is equal to 1.43 [W/m^2 K] and its constructive layout is shown in the Table 4 of Appendix A. Likewise, this façade is equipped with a window of dimensions 1.16×1.08 m. In the present study, this façade is considered as the reference façade and its energy performance is compared to that of the OVF under analysis to reach conclusions about the potential energy savings that OVF provides.

The OVF is placed on the south-facing façade of the Cell 1, Fig. 1(a), and is the result of adding a ventilated facade system with opaque skin to a façade with the same constructive characteristics as the

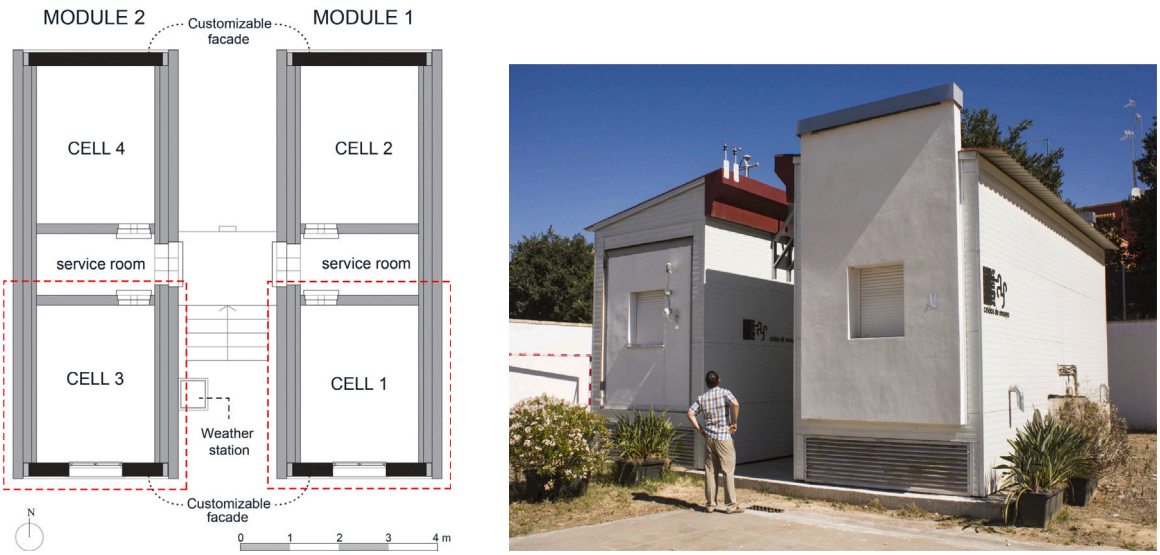

Fig. 1. (a) Floor plan of the test cells. (b) Test cells.

energetically obsolete south-facing façade of Cell 3. and keeping the window in its previous position. The layout of the OVF is shown in Table 5 of Appendix A, being now the transmittance of the inner wall equal to 0.56 [W/m^2 K].

The air duct is laterally closed with the same materials as the outer skin and connects to the outside by means of a horizontal inlet opening placed at the bottom of the duct, the thickness of which is 0.1 m, i.e. the thickness of the ventilated chamber. This opening has a system of grills that can be opened and closed, so that the resulting opening surface, when the grills are open, is 50% of the total surface of the base of the ventilated chamber. Another 0.1 m wide vertical opening is located at the top of the OVF on the same axis as the outer skin, and it is equipped with a protection about 20 cm over the exterior side, providing protection against rain.

The 50% reduction of the inlet opening area may raise the question of whether the ventilation of the ventilated chamber is guaranteed or not. In this regard, in the previously mentioned paper from Fantucci et al. [15], the thermal performance of different ventilated façade configurations was evaluated through an extensive experimental campaign under summer conditions. Among these configurations, three ventilation grills opening ratios with respect to the total opening were considered: 33%, 61% and 100%; measurements showed that the impact of the grills opening ratios was moderate on the energy performance of the facades, concluding that the decrease in the daily heat gain reduction capacity of the OVF is about 5% going from 100% to 33% of the grills opening ratio, and is less than 2% going from 100% to 61% of the grills opening ratio. Regarding the air velocity in the ventilated channel, and the associated ventilation capacity, a direct correlation was observed between the grills opening ratio and the air velocity: for the opening ratio of 100% velocity ranged between 0.60 and 0.70 m/s, while for the opening ratio of 61% velocity ranged between 0.50 and 0.60 m/s, and for the opening ratio of 33% velocity ranged between 0.35 and 0.45 m/s. These results can be interpreted as the considered variations of the grill opening ratios affect the velocity inside the ventilated channel, but allow good ventilation, as can be seen from the small variation in the daily heat gain reduction capacity of the OVF observed for the different grill opening ratios.

Likewise, in [18] the thermal behavior of rainscreen ventilated façades under typical Mediterranean summer weather conditions was investigated experimentally by using a large-scale test building. In this work, inlet and outlet grills opening partially closed are studied, although the value of the opening ratio is not provided. It was found that in the case of partially opening grills ratios the air velocity in the ventilated cavity decreases compared to fully open inlet and outlet grills, resulting in an increase in heat flux through the inner wall. However, the reported values of air velocity in the case of partially open grills ranged from a minimum of 0.38 m/s to a maximum of 1.23 m/s, implying that the air flow rate is guaranteed inside the ventilated chamber.

Finally, to refer to one last work, in [26] an OVF with a configuration of grills as used in the present paper was exhaustively analyzed, both experimentally and numerically; from the obtained monitored and numerical data it was observed that the air velocity in the inlet region of the ventilated channel is able to reach values above 0.3 m/s, which allows to guarantee the air flow rate for the ventilation of the chamber.

Thus, in light of previous research, it can be asserted that the 50% grill opening ratio considered in the experimental configuration used in the present paper is enough to allow ventilation of the ventilated cavity.

Regarding the other elements of the envelope of the Cells, the floor slab, the roof and the east and west walls are composed of highly insulated white panels with a global thermal transmittance value equal to 0.05 W/m^2 K. On each cell roof is installed a sloping plate of galvanized corrugated sheet metal panels that form a ventilated space. The north interior walls of Cell 1 and Cell 3, adjacent to the service area, are made of a 100 mm thick sandwich panel, whose thermophysical values are the same as those of the sandwich panels used in the east and west walls. The layout and characteristics of these elements of the cells envelope are described in Table 6 in Appendix A.

2.2. Façade modeling

The analysis performed here is based on the calculation of the energy flux through the OVF when different values of the dimensions and physical variables of the elements that make up the OVF are considered.

To compute the energy flux through each configuration of the OVF, the three-dimensional model introduced in [26] is used to compute the velocity and temperature of the air within the ventilated channel and the heat conduction through the solid elements of the OVF. In the ventilated channel, the equations governing air flow and transport temperature are the Navier–Stokes thermodynamic equations with a Boussinesq approximation for buoyancy. These equations are completed with a modeling of the turbulence using the RNG $\kappa - \varepsilon$

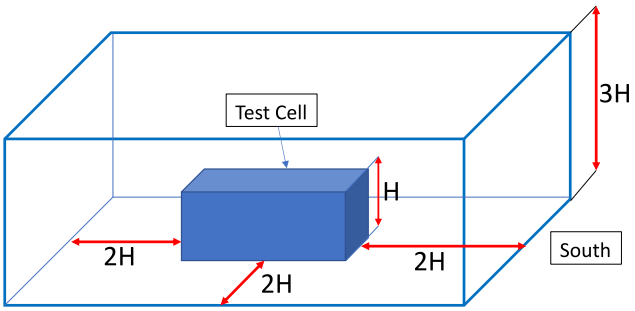

Fig. 2. Scale-free view of the 3D computational domain.

model following [38] where it is asserted that this turbulence model performed better than other turbulence models for calculating heat transfer in the case of an air flow with low velocity zones.

The use of the Boussinesq approximation for buoyancy has been widely used in the context of ventilated façades. Some works that use this approximation are cited below. In [39] the Boussinesq approximation is used in combination with $\kappa - \varepsilon$ and $\kappa - \omega$ models for the turbulence; for the OVF configurations analyzed, the differences found between the simulated surface temperatures and the experimental data are lower than 5% for both turbulent models whilst for the velocity of air in the ventilated chamber it was found that it ranges 6–15% higher than the experimental values; according to the obtained results, the simulation model implemented in the CFD environment was considered validated. In [11] the Boussinesq approximation was used to model buoyancy effects in the study of the thermal and fluid dynamic behavior of open-joint ventilated façades; experimental validation showed goof fittings in temperature and velocity profiles among simulated an measured data.

On the other hand, Li et al. [40], presented a study in which a model was calculated by theoretical analysis and by CFD simulation using the Boussinesq approximation; authors concluded that the results obtained showed less accurate predictions that those obtained from the Incompressible-Ideal-Gas model. This implies that the use of the widely used Boussinesq approximation to deal with natural convection should be used with caution and whenever possible be validated experimentally.

Taking these issues into account, an extensive validation process was carried out in [26] to ensure the good accuracy of the numerical model used in the prediction of the energy performance of the ventilated façade under study. The experimental measurements allowed to conclude the validation of the numerical model used, which included the use of the Boussinesq approximation to model buoyancy effects, although, as in the work by Buratti et al. [39], the simulated values for temperatures show higher accuracy than for velocities.

The heat transfer through the inner wall and the outer slab of the OVF are modeled by the heat conduction equations.

The boundary conditions for the air flow are non-slip condition on all the solid surfaces whilst the air velocity incoming to the computational domain are computed by using the air velocity from weather data. To calculate the air velocity at the inlet of the air duct, a part of the external environment around the cells is incorporated into the calculation domain, as shown in Fig. 2. In the upper part of the computational domain, the slip condition is imposed and, finally, free outflow on the remaining boundary surfaces. For temperature, the boundary conditions on solid surfaces are given by the equations of energy balance on each surface.

The numerical resolution of the OVF model was performed by using a 3D Finite Element discretization of the thermodynamic equations for the air flow and of the equations of heat conduction through the solid elements of the OVF. The computational code was built by using the free software FreeFem++ [41] that is a partial difference solver based on the Finite Element Method (FEM) developed by the French Institute National de Recherche en Sciences et Technologies du Numérique. More details of the used simulation model and its numerical resolution can be found in [26].

2.3. Model validation

The OVF model was validated through an exhaustive validation process that included the use of monitoring measurements from an extensive experimental field campaign carried out during the aforementioned spring, summer and winter time intervals. The monitoring equipment used in the validation process is detailed in Appendix D.

In the validation process, the calculated values of the temperatures of the OVF surfaces, the temperature and velocity of the air flow into the air duct, as well as the heat transferred through the OVF to the indoor space were compared with the monitoring values.

The validation analysis was performed following the broadly recognized guidelines for evaluating the precision of building energy models (BES) as set forth by ASHRAE Guideline 14-2014 [42], the International Performance Measurement and Verification Protocol (IPMVP) [43], and the Federal Energy Management Program (FEMP) [44].

This validation process allowed to assert the accuracy of the numerical method used to simulate the energy performance of the OVF.

A summary of the results of the validation process can be found in Appendix B, while a detailed description of this process can be found in [26].

3. Optimization analysis methodology

3.1. Façade configurations for the parametric optimization analysis

The parametric analysis of the energy performance of the OVF has been carried out considering the variations of the different façade design parameters listed below:

- the ventilation grille opening protocol considering two cases: closed and opened.
- the air channel thickness (from 0.02 m to 0.3 m).
- the outer surface solar absorptivity (from 0.1 to 0.9).
- the OVF outer sheet diffusivity (from −30% to 30% of the initial value).
- the insulation thickness (from 0.02 m to 0.2 m).
- the air channel height (one and two floors).

To investigate the impact of variations of each parameter on the thermal performance of the OVF, the heat transferred through the OVF to the interior space was calculated by varying the parameter under study, and keeping the rest of the parameters unchanged in the initial configuration of the OVF described in Section 2.1. Finally, once the best value for each parameter was determined, the yearly heat flux and associated savings were calculated for the configuration resulting from the application of these optimal parameter values.

3.2. Heat flux computation and performance metrics

This section describes the procedure followed to compute the yearly heat flux (YHF) through the OVF and the metrics and variables used in the OVF parametric energy optimization process.

The variable to be optimized is the yearly total heat flux through the OVF, so the lower this flux, the more energy efficient the OVF is considered to be and the value of the design parameter that provides the minimum amount for YHF is considered the optimal value for this parameter.

To compute YHF the climatic data of a representative day of each season have been used. The climatic data for this representative day of each season were calculated by computing for each weather variable its mean value over the entire season. This typical day can be

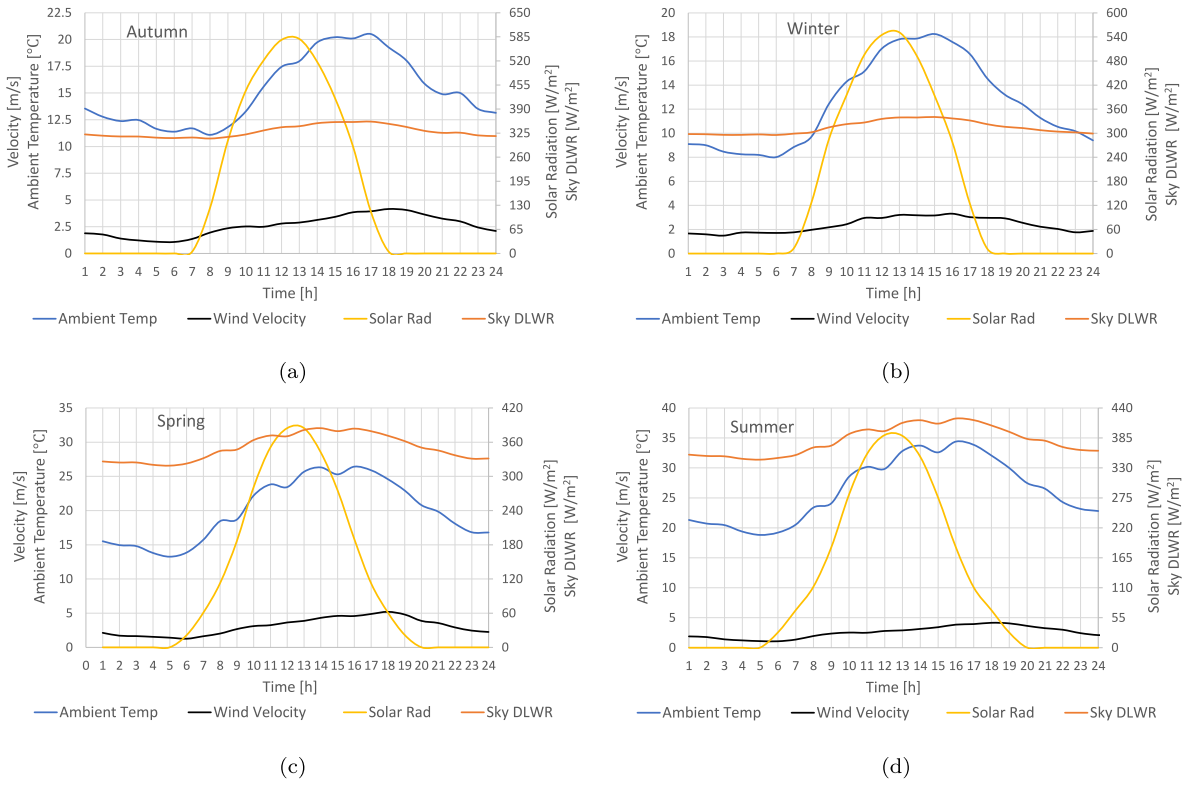

Fig. 3. Climatic variables for seasonal representative days: (a) Autumn; (b) Winter; (c) Spring; (d) Summer.

considered as a valid and fair representation of the season for energy computations [17].

To calculate YHF for every seasonal representative day, the transient nature of the heat transfer through the wall was taken into consideration and then, based in [45], the expression used was:

$$q = \frac{1}{A(W)} \int_{t_{ini}}^{t_{end}} \left(\int_{W} h_{(c,r)} |T_W - T_{ind}| \right), \tag{1}$$

where W represents the inner surface of the wall where the OVF is installed, $A(W)$ is the area of W, T_W the surface temperature on W, T_{ind} the indoor air temperature, $h_{(c,r)}$ the mixed convective-radiative heat transfer coefficient between W and the indoor ambient and $[t_{ini}, t_{end}]$ is the time interval for which the total heat flux q is calculated, in our case a typical day for each season. Here, the value of $h_{(c,r)}$ is taken equal to 8.29 W/(m^2 K) in accordance with ANSI/ASHRAE Standard 140 [46].

To compute q for each seasonal representative day, a four-day warming interval was used in all energy calculations in order to consider inertial thermal effects. More warming days do not provide substantial changes in energy calculations, with less than 0.3% difference in energy results for a heating interval of one-week

Finally YHF is calculated by using the values of q obtained from Eq. (1) extended to all days of each season and adding the values obtained for the four seasons [17].

The calculation of the heat flux through the OVF is used in combination with the yearly energy saving percentage (YESP). This parameter is defined as

$$\text{YESP} = \frac{\text{YHF} - \text{YHF}_{Ref}}{\text{YHF}_{Ref}} \cdot 100, \quad [\%]. \tag{2}$$

where YHF_{Ref} represents the yearly heat flux for the original energy obsolete façade named as the reference one. Using the criterium of energy savings, the greater the YESP, the more energy efficient is the OVF configuration and the one that provides the maximum value of YESP is considered the optimum configuration.

To finalize the optimization analysis, once the optimal value that provides the lowest YHF for each design parameter has been obtained, the values of YHF and YESP are calculated for the constructive OVF configuration resulting from the combined use of the optimal values for each parameter.

3.3. Indoor conditions

The goal of this work is to draw conclusions about the OVF configurations that minimizes the heat transfer through the OVF and the associated savings when compared to an energy obsolete reference façade considering that indoor temperatures are into the comfort range. For this, following the approach introduced in [47,48] and [49], the interior zone of the tests cells is modeled as a test zone assuming that the envelope of the test cells is adiabatic except for the customizable South wall. For this purpose, a continuous mode of the conditioning system is assumed with an indoor set-point temperature set at 21 °C in winter, at 25 °C in summer and, finally, set at 23 °C in spring and autumn. These values have been proposed taking into account the comfort temperature ranges established in the Spanish regulations for conditioning equipment in buildings (RITE) [50].

3.4. Climatic data

In Figs. 3(a), (b), (c), (d), the exterior temperature, the southern solar radiation, the sky downward long-wave radiation, and the wind velocity are shown for the representative days of each season in Seville used in the computations. These values were obtained based on data from the Spanish State Meteorological Agency [51] and the Energy Plus Weather (EPW) file for the city of Seville. The values of the different weather variables can be considered as typical of the Mediterranean climate. As can be seen in these figures, this climate is characterized by high values of the solar radiation for the whole year, and temperatures can be considered as mild during winter, as moderate during spring and autumn, and as hot in summer. In view of these characteristics, the climate of the region is classified as Mediterranean Csa in accordance to the Köppen–Geiger climate classification.

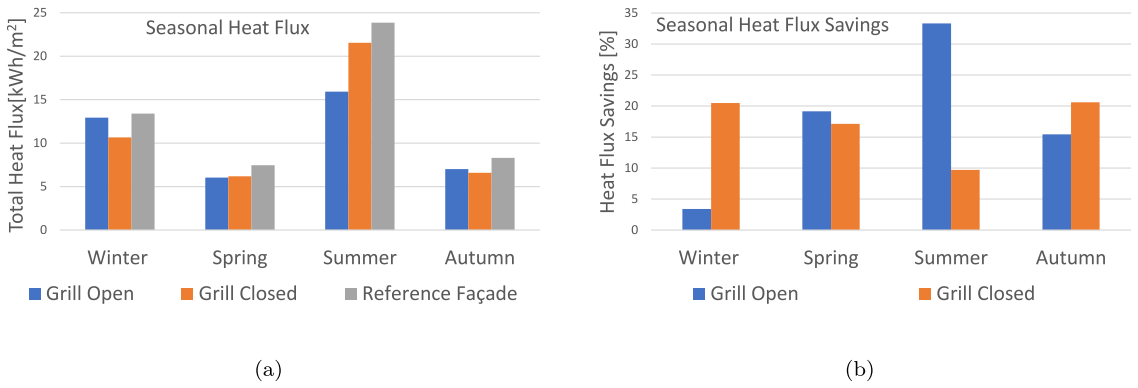

Fig. 4. Grills opening protocols: (a) seasonal heat flux; (b) seasonal heat flux savings.

4. Results and discussion

In this section, the results of the YHF and YESP computations for each OVF configuration described in Section 3.1 are shown. As already mentioned, the goal of this research is to find conclusions about the OVF configuration that minimizes the heat flux through the OVF for the whole period of a typical climatic year and thus, maximizes the energy savings for the entire year. The YHF and YESP values obtained for each OVF configuration are presented in the following sections.

4.1. Ventilation grills opening

In this section, the impact of the ventilation grills opening protocols on the heat flux through the OVF and associated savings are analyzed. Two cases are considered: grill opened and grill closed.

Since the open grill allows for free circulation of air throughout the ventilated chamber, in this case a higher convective exchange is expected between the surfaces facing the duct and the air flowing along this channel. This can result in a cooling of these surfaces if the air entering the channel has lower temperatures, and therefore in a reduction of the cooling load; but if the air entering the channel has a very high temperature, this reduction may be very low or non-existent [25]. However, in winter, the entry of cold air into the ventilated chamber can cause an increase in the heating load, in addition to the increase in this load due to the solar radiation blocking effect produced by the outer layer of the OVF.

In contrast, when the grill is closed, in winter there is no cold air intrusion and the ventilated chamber can perform as an extra layer of thermal insulation and then reduce the heating load, while in summer the absence of ventilation can increase the cooling load compared to the open grill case.

Thus, taking into account the opposite thermal performance produced by both protocols throughout the year, it is necessary to evaluate the heat flux through the OVF for every season in order to draw conclusions about the best protocol for each season, so that the combination of the best protocol in each season yields the optimum protocol for the whole year.

In Fig. 4(a) the seasonal total heat flux is shown for the OVF with the two studied protocols of open and closed ventilation grille and for the reference façade. It can be observed that in summer, the OVF with open grill is able to strongly reduce the heat flux compared to the reference case. This reduction, as it is shown in Fig. 4(b), is equal to 33.3%, value that is in accordance with results supported by literature where for hot areas and the summer season in [8] energy savings between 22% and 38% are reported for fixed typical climatic summer conditions for some suitable OVF configurations with a channel thickness similar to the one used in the present work in the initial configuration. On the other hand, in [7] heat flux reductions for a day of summer range between 7% and 27.5% in function of the air channel width, and in other works the heat reduction typically is close to 40% for OVFs without window openings [9,10,12,13]. It must be outlined that most of the referenced works are focused in OVF without window openings, and the heat reduction is assessed for specific summer days or static weather conditions, while here the heat reduction is computed for a whole representative day of the season and for an OVF with windows openings, so, the results presented here should not be directly compared with previous results in the literature, except to determine a qualitative behavior that can be stated to be similar in terms of heat flux reduction values.

For its part, the OVF with closed grill is also able of reducing the heat flux through the OVF, although now, this reduction is equal to 9.7% and therefore much lower than the reduction for the open grill case. This poor reduction can be related with the no possibility of transporting the heat energy of air to the outside of the ventilated chamber and, in this way, to lower the temperature of the walls facing this chamber; nevertheless, the ventilated chamber itself acting as a thermal insulation layer, the outer shield that protects the inner wall against solar radiation, and the extra insulation layer with which the OVF is equipped, are able to produce the reduction in heat flux mentioned earlier.

In contrast, in winter, the best performance in terms of heat flux reduction is found for the OVF with the closed ventilation grill, which yields a percentage saving equal to 20.5%, whilst the reduction reached by the OVF with open ventilation grill is equal to 3.4%. The reason for these results is based precisely on the thermodynamic behavior of both cases described above. Thus, in the cold season, mainly due to the intrusion of cold air inside the ventilated chamber have the opposite results in the heat transfer through the OVF described above, whereas in the cold season, mainly because of the entrance of cold air inside the ventilated chamber, have the opposite results on the heat transfer through the OVF.

In the intermediate seasons, spring and autumn, the heat fluxes are much lower for all the cases. However, the OVF is again able to reduce the heat transfer in both seasons, this reduction being up to 20%, which is a significant reduction, although, it should be noted that these percentage reductions apply to relatively low values of heat flux for these seasons as can be seen in Fig. 4(a).

From the analysis of the results presented in Fig. 4, it can be concluded that the OVF with open ventilation grill has significantly better performance compared to the closed ventilation grill only in the summer season, although the difference in this case is very high in favor of the open case. In light of these results, in order to select the most efficient grill opening protocol, it is necessary to evaluate the heat fluxes and its reduction for the whole year for both grill protocols, results that are presented in Fig. 5 and Table 1.

In Fig. 5(a), the yearly heat fluxes are shown for the two grille protocols, closed and open, and for the reference case. As can be seen, the open protocol for the grille inlet gives the lowest value of YHF,

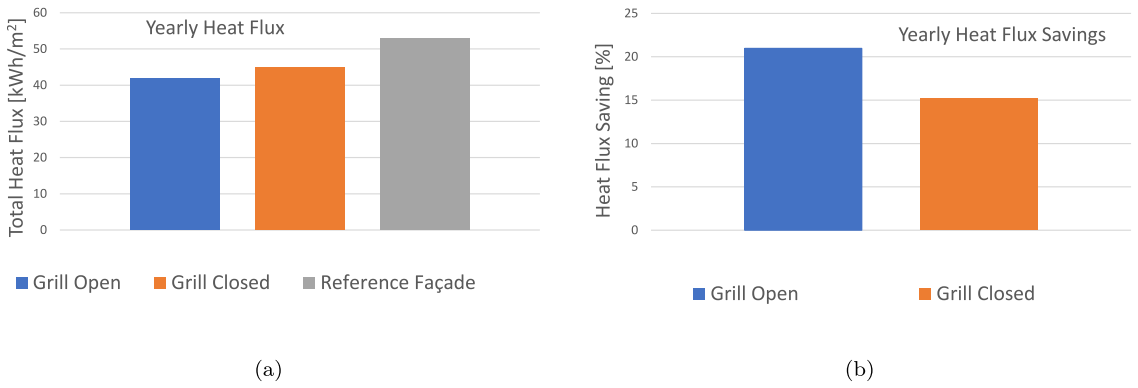

Fig. 5. Grills opening protocols: (a) yearly heat flux; (b) yearly heat flux savings.

Table 1
Yearly heat flux for the OVF and associated savings for the different grills opening protocols.

	Grill closed	Grill open	Grill combined	Reference case
Yearly heat flux [kWh/m^2]	44.96	41.89	39.17	53.01
Yearly load savings [%]	15.17	20.96	26.09	–

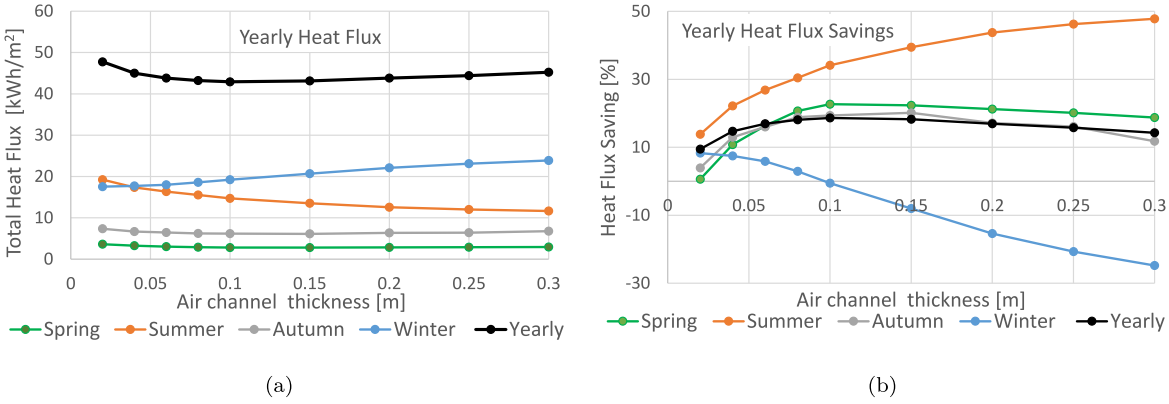

Fig. 6. Different thickness values of the air channel; impact on: (a) yearly heat flux; (b) yearly heat flux savings.

although the case with closed grille yields too a lower value of YHF than the reference case according to the discussed seasonal results for the heat flux. The yearly percentage savings for the open grill is equal to 20.96% and for the case with the closed grill is equal to 15.17%, that confirms the relevance of this kind of retrofitting measure and the best performance of the OVF with the open grill when compared to the closed case as can be seen in Table 1.

It is noteworthy to observe that once the heat flux is computed for each season and each protocol, taking into account that the lower values of the total heat flux are given in winter and autumn for the grill closed protocol and in spring and summer for the grill open protocol, a new protocol could be defined, named the combined one, choosing for each season the grill protocol that produces the minimum values for the heat flux through the OVF. The savings for this protocol are shown in Table 1 where as can be expected this combined protocol is the most efficient to decrease heat transferred across the OVF. However, the effective implementation of this optimum protocol requires some kind of mechanic control of the grille aperture that can increase the costs of installation of the OVF and can make this option economically unprofitable. Therefore, a careful cost-effectiveness analysis is necessary in order to establish its suitability before choosing this option as the best.

In the following sections, to study the impact of varying the different characteristics of the OVF analyzed in the optimization analysis, only the results for the open grill protocol are shown for the sake of brevity.

4.2. Air channel thickness

In this section, the yearly heat flux and the yearly heat flux savings for different air channel thicknesses are computed, and the values obtained are shown in Fig. 6. The configuration of the OVF is the original one and only the thickness of the ventilated chamber is varied from 0.02 m to 0.3 m (around the original value of 0.1 m).

As can be seen in Fig. 6(a) in summer the heat flux through the OVF decreases as the air chamber thickness d increases, being the decrease of YHF specially marked for values of d lower than 0.10 m tending to a stabilization of the YHF for values of d greater than 0.2 m. Therefore, the decrease of the YHF for 0.1 m$< d <$ 0.15 m is close to 21% whereas for 0.2 m$< d <$ 0.3 m is about 4%. This implies a heat flux saving that increases as d increases, with a high increase until d reaches values between 0.1 and 0.2 m, tending for values greater than this interval to a much slower growth as can be observed in Fig. 6(b). These facts for the heat flux and associated savings3/4 are in accordance with the findings reported in [8].

On the other hand, regarding the behavior of the heat flux in the winter season in can be observed in Fig. 6(a) that the heat flux through the OVF responds in an opposite way that in summer to changes in d. Thus, it can be observed how the increase of d produces an increase in the heat flux due to the increase of the cold air flux rate inside the channel in such a way that for values of d lower than 0.1 m the OVF is able to reduce the heat flux through the OVF but, once this value of d is exceeded, savings become increasingly negative until for values

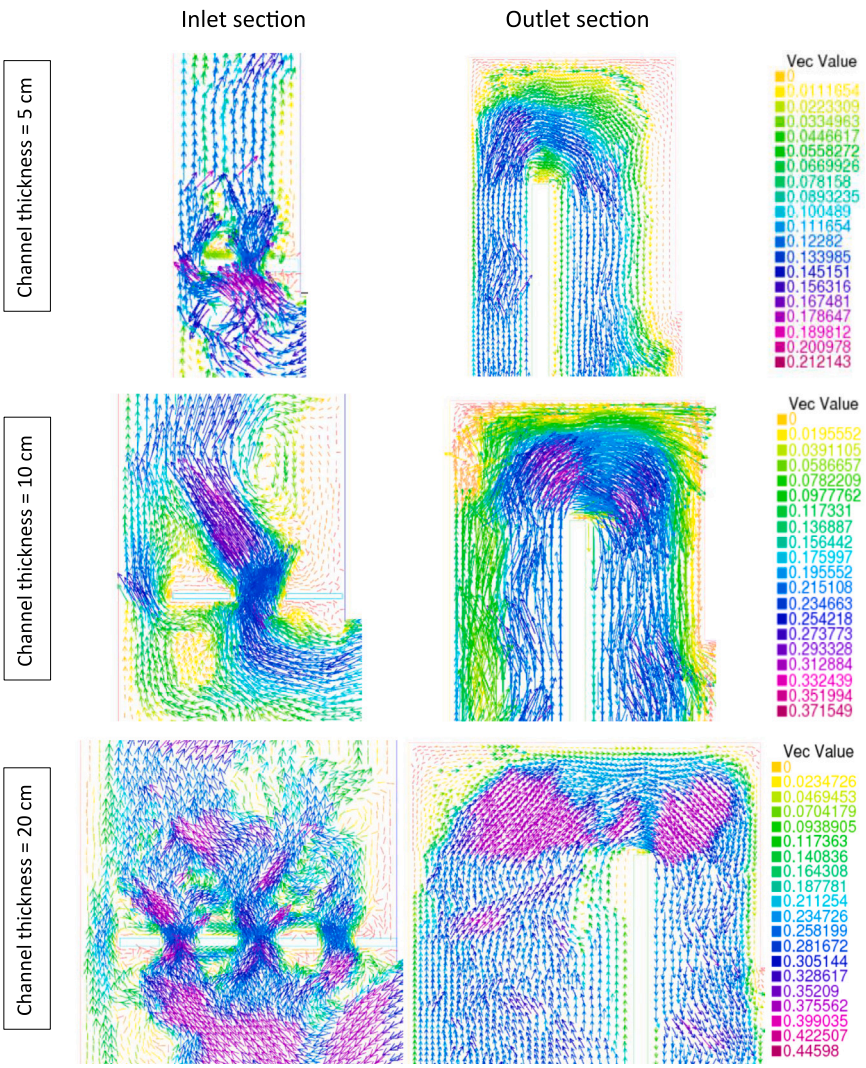

Fig. 7. Velocity fields in the areas of the inlet and outlet openings for the vertical section in the center of the lateral region of the ventilated chamber next to the window (line of sensors TA2, TA3 and TA4 in Fig. 18), for different values of chamber thickness. Velocity magnitude (Vec Value) are shown.

of $d = 0.3$ m savings reach a value close to −40%, Fig. 6(b), showing a pattern of behavior like that reported in [7,11].

For the intermediate seasons, as can be seen in Fig. 6(a), the values of the heat flux are lower than in summer and winter. In spring, as shown in Fig. 6(b), for all the values of d positive savings are obtained that increase with increasing d, this increase being stronger until d reaches values between 0.1 and 0.15 m, being the increase more smoothly for values of d greater than 0.15 m. In autumn, savings behavior follows a pattern opposite to that of spring. This could be an indication that in these seasons, the ambient temperature does not greatly affect the energy transfer through the OVF, which is highly protected against thermal losses by the insulating layer that is able, in a framework of warm ambient temperatures, to reduce the heat transfer through the OVF for all the considered values of d.

Regarding the yearly total heat flux, in Fig. 6(a) shows how the behavior of this flux over the seasons is affected by different values of d. Thus, for $d < 0.1$ m, the YHF follows a decreasing pattern associated with increasing energy savings, Fig. 6(b); once this value is reached, little change is observed in the YHF with a slight increase for $d < 0.115$ and, correspondingly, in the associated savings, until for values of d above 0.15 m, the YHF tends to increase again and the savings tend to decrease both smoothly, indicating that for these values of d the winter heat losses predominate over the summer cooling effect.

In conclusion, on the basis of the preceding discussion, the values of d equal to 0.1 m produce the lowest YHF and, consequently, the greatest heat transfer reduction through the OVF with window openings in the considered climatic framework.

On the other hand, it should be noted that an increase in the thickness of the air channel entails an increase in construction complexity, which will translate into a notable increase in execution costs [13]; this may advise limiting the thickness to values where the rate of decrease of the heat flux becomes already small.

The yearly heat flux through the OVF and the associated yearly heat flux saving compared to the reference case are shown for the different air channel thicknesses considered in Fig. 6.

In Figs. 7 and 8, velocity fields are shown for different thicknesses of the ventilated air space at noon on a typical summer day. For the thickness values shown, 5, 10 and 20 cm, a slight increase in velocities is observed as the thickness increases, which is in agreement with what has been observed in the literature for this range of thickness values [8]. For the temperature field, it is observed that as the thickness of the ventilated chamber decreases, an increase in the temperature of the air circulating through the chamber is observed, which translates into a loss of its cooling capacity, as also referred to in the previous reference and is illustrated in Fig. 6.

4.3. Solar absorptivity

To assess the impact of changes of the solar absorptivity on the energy performance of the analyzed OVF, this value is introduced

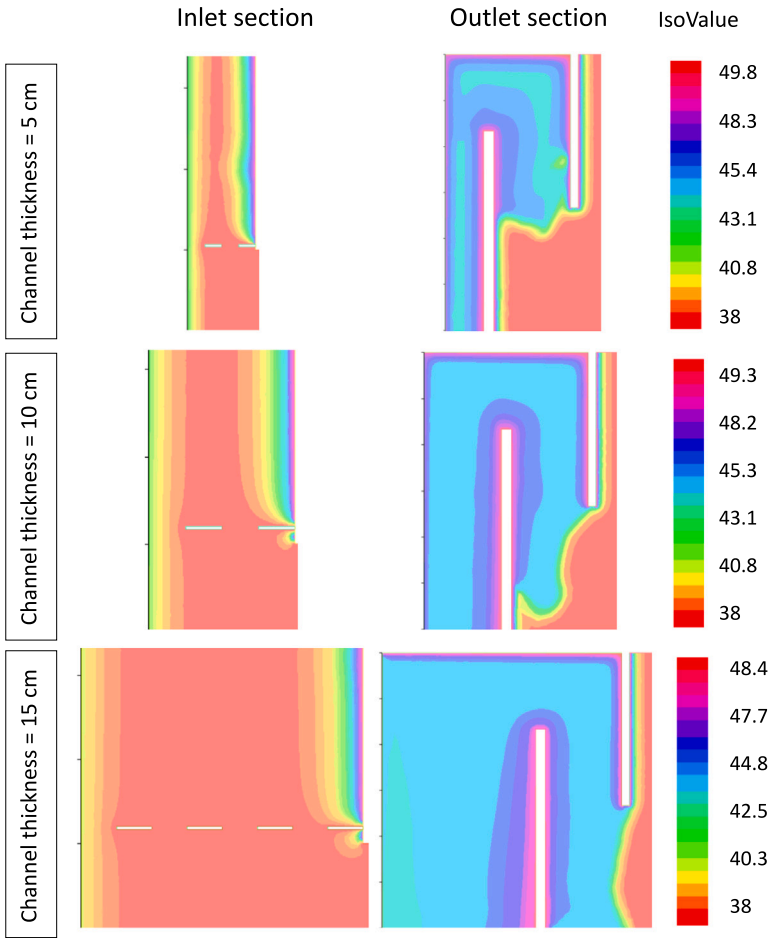

Fig. 8. Temperature fields in the areas of the inlet and outlet openings for the vertical section in the center of the lateral region of the ventilated chamber next to the window (line of sensors TA2, TA3 and TA4 in Fig. 18), for different values of chamber thickness. Temperature isovalues (IsoValue) are shown.

directly as a parameter in the numerical model used. In the present research, the values considered for the solar absorptivity of the external surface of the OVF outer layer range from 0.1 to 0.9 with steps equal to 0.1.

In Fig. 9(a), the YHF for different values of the outer surface solar absorptivity is displayed as well as for the reference case. For practically all the values of solar absorptivity considered, the heat flux through the OVF is lower than through the reference façade. Only for values of solar absorptivity equal to 0.1 and 0.9, a slightly higher value of the YHF for the OVF is observed when compared to the reference case.

As can be seen in Fig. 9(a), the annual heat flux has a convex behavior reaching its minimum for a value of solar absorptivity equal to 0.4, and consequently a maximum of savings for this value. This fact can be explained as follows: for the lowest value of solar absorptivity, low values of absorbed solar energy predominate, resulting in an increase of the heat flux in the cold season towards the outside and an overall increase of the annual heat flux; then, as solar absorptivity increases, the penalty effect in winter is progressively reduced until YHF reaches its minimum for solar absorptivity equal to 0.4, and then the growth of this parameter implies an increase of the heat flux over the summer that produces the increase of YHF for all values of solar absorptivity higher than 0.4, so that for the solar absorptivity range between 0.4 and 0.9, the higher the value, the higher the YHF.

In Fig. 9(b) the savings for the YHF are shown. These savings range from a minimum negative value close to −3% for a solar absorptivity equal to 0.1 to a maximum value close to 21% for a solar absorptivity equal to 0.4. When this absorptivity value is exceeded, the saving gradually decreases to a value of about −6% for the highest absorptivity value equal to 0.9.

Thus, taking into considerations the results of this section, it can be stated that the optimum value for the solar absorptivity for the present case study is equal to 0.4.

4.4. Thermal diffusivity of the outer sheet

Taking into consideration that changes in the value of the thermal diffusivity α of the outer sheet can influence the heat exchange through the OVF, in this section the impact of varying α on the YHF is analyzed. For this, α is modified from a minimum of −30% to a maximum of 30% of its original value given by the physical properties of the outer sheet shown in Table 5.

Fig. 10(a) shows the YHF for different values of the outer sheet thermal diffusivity α. It is possible to observe that the lower value has α the lower value has YHF, in such a way that a −30% decrease of α gives a YHF value equal to 39.57 kWh/m^2 versus a YHF equal to 41.89 kWh/m^2 for the original OVF, i.e, a reduction in heat transfer of about 25.33%, while a 30% increase of α yields a YHF value equal to 58.07 kWh/m^2, equivalent to an increase of heat transfer equal to 9.55%.

As conclusion of this analysis for α, it is possible to state that materials used in the coating layer with a lower the thermal diffusivity provide best results in terms of heat flux through the OVF, which is in accordance with the results from [9], although newly, the results of this last work have been carried out for stationary assumptions that reproduce the conditions of one hour of daylight on a summer day,

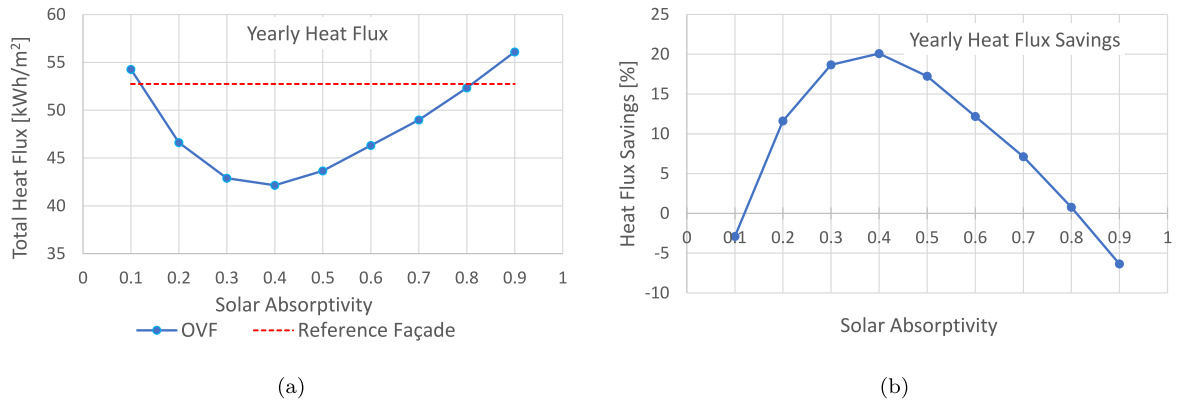

Fig. 9. Different solar absorptivities of the external surface; impact on: (a) yearly heat flux; (b) yearly heat flux savings.

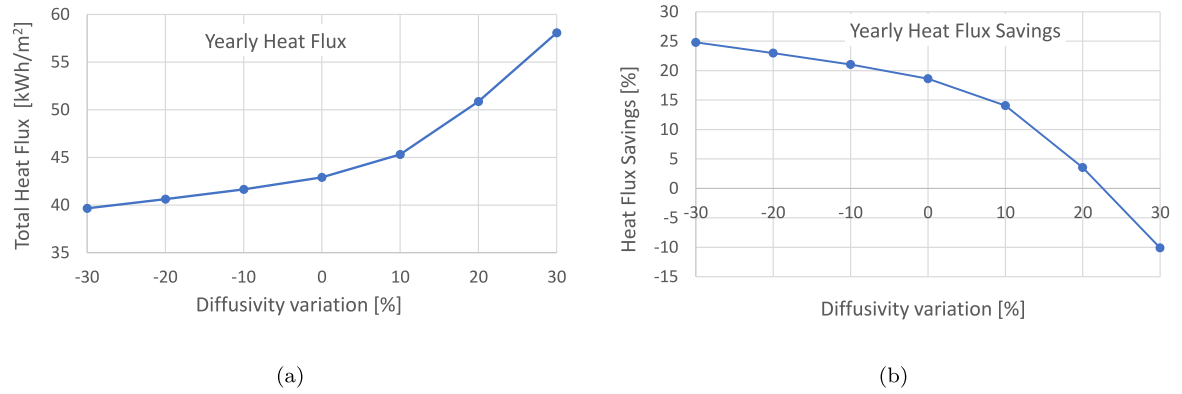

Fig. 10. Different thermal diffusivities of the external sheet; impact on: (a) yearly heat flux; (b) yearly heat flux savings.

while in the present work the analysis has been carried out for non-stationary conditions extending over representative days of each season of the year.

4.5. Insulation thickness

In this section, the impact of varying the thickness of the insulation layer on the heat flux through the OVF is assessed. The insulation layer thickness values range from 0.02 to 0.2 m and the corresponding values of the resulting YHFs are shown in Fig. 11(a). As expected, taking into account the role of the insulation layer in blocking the heat flux, the thicker it is, the lower the heat flux through the OVF. As can be observed in the figure, the decrease of the YHF is more marked for insulation thickness values between 0.02 m and 0.12 m, ranging the YHF from a value of 57.54 kWh/m^2 to a value of 36.41 kWh/m^2 than means a percentage decrease of 28.31%, while the decrease for thickness values between 0.12 m and 0.20 m goes from 36.41 kWh/m^2 to 32.58 kWh/m^2 that is a percentage decrease of only 7.24%.

The yearly heat flux savings for the different values of insulation layer thickness analyzed are shown in Fig. 11(b). According to the behavior of the YHF displayed in Fig. 11(a), a very marked growth in savings can be observed for thickness values up to 0.12 and a much slower growth of savings for thickness values above 0.12 m. In Fig. 12 can be observed as the rate of yearly heat flux decrement is very high for values of insulation thickness lower that 0.06 m, a decrement rate something lower for values of the thickness between 0.08 and 0.12 m and then, for values greater than or equal to 0.15 m, the decrement rate tends to stabilize taking values lower than 0.5 kWh/m^2 per cm of increase of the insulation thickness.

From this results is obvious that increasing the thermal insulation layer of the OVF produces a lower heat exchange between the interior and the exterior of the building, but observing the decrement rates of YHF that are obtained for values of the insulation thickness it could be taken a value for the insulation layer thickness between 0.6 and 0.1 m as the one than provides the more reasonable balance between cost of materials and energy cost savings, although this should be analyzed through a cost-effectiveness analysis that is out of the scope of this research.

4.6. Ventilated façade height

Two phenomena are observed when the ventilated façade height is increased: in the presence of solar radiation, both the velocity and the temperature of the air flowing inside the channel tend to increase as the air rises up the channel, as observed in [15]. Thus, according to previous research, increasing the height of the façade also increases the air flow rate in the cavity, resulting in an improvement of the energy performance of the ventilated façade [11,27].

In the present research, to study the effect of the height on the heat flux through the OVF, the original OVF is modified by adding and modeling a second floor with the same characteristics as the initial OVF. Likewise, an intermediate separation space is added to model the slab of separation between both floors of the building. A sketch of the considered OVF with the modified façade height is shown in Fig. 13(a). The OVF is divided in zones to describe the results: zones 1,2,6,7 and 8 belongs to the first floor, zones 3 and 9 correspond to the slab of separation between the first and the second floor, and finally, zones 4,5,10,11 and 12 belongs to the second floor. It should be noted that the presence of the two windows causes a lateral displacement of the air flow around both windows opening inside the ventilated chamber so that the thermodynamic behavior of the air flux is symmetrical in the lateral zones as can be seen in Fig. 14(a) and (b) and it was shown in [26]. This is the reason why the lateral zones have the same names.

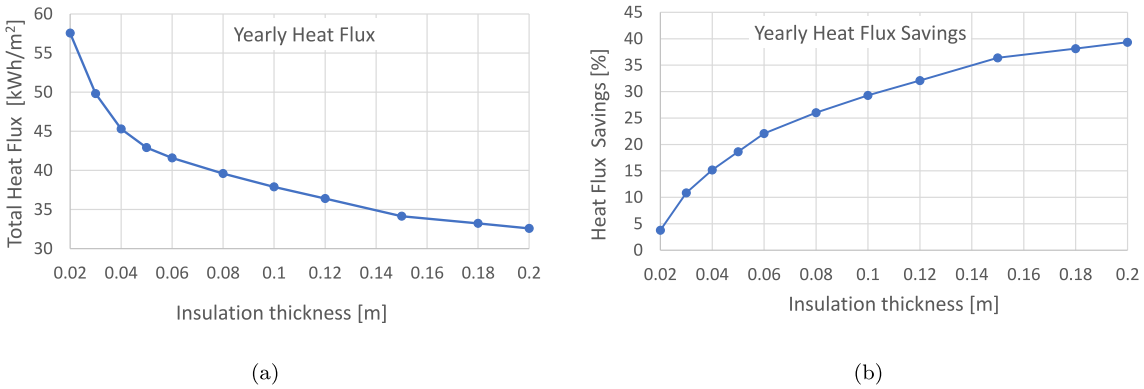

(a) (b)

Fig. 11. Different thickness of the insulation layer; impact on: (a) yearly heat flux; (b) yearly heat flux savings.

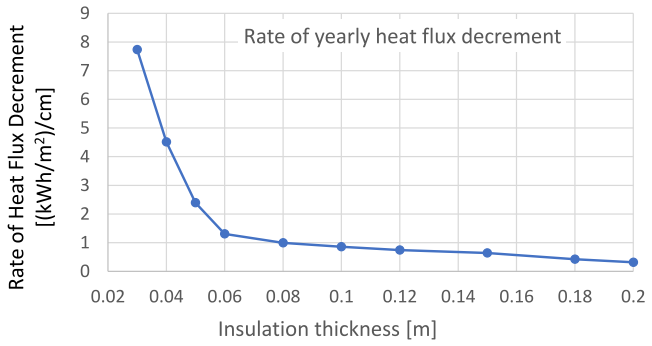

(a)

Fig. 12. Rate of yearly heat flux decrement.

In Fig. 13(b) the 3D mesh of the ventilated chamber used in the computations is displayed.

In Figs. 14(a) and 14(b), the velocity and temperature fields of the air in the middle section of the ventilated chamber are displayed at noon of the typical winter day. On the other hand, in Figs. 15(a) and 15(b), the air cavity velocity and temperature are displayed as a function of the channel height for a winter and a summer typical day. Based on these figures a similar pattern can be observed for both seasons: on one hand, velocity in zones 7 and 11 reaches the highest values according with the observed in [26] at the same time that a slight increase of velocities is found for each zone of the second floor when compared with the equivalent zone at the first floor height, that is according with the findings from [15] where an increase in the air velocity is reported when the height of the channel is increased; on the other hand, the temperature of the air increases as the channel height increases for both seasons being this increase most marked between the zones 6 and 7 due to in zone 6 the air is still most affected by the incoming air temperature while from zone 7 the temperature has a slower increase of almost linear character.

Regarding the heat flux through the OVF, two values of the YHF are computed: one for the first floor of the OVF that coincides with the façade analyzed in the previous sections and a second value of the YHF for the added second floor. This is made by using Eq. (1) but using now the values of T_W as the surface temperature on the inner surface W of each floor and T_{int} as the indoor air temperature of each floor. In order to draw conclusions about the heat transfer at the second floor that allows for comparison with the values of YHF obtained for the first floor, T_{int} is taken equal in both floors according to the comfort temperature values specified in Section 3.3.

In Fig. 16(a) and Fig. 16(b), the total heat flux and associated savings for each season are displayed for the first and second floors of the OVF and for the reference case façade. It can be observed that in summer, the ventilated façade at the first floor height performs better than the one at the second floor, and, as it is shown in Table 2, this difference is a 2.76% lower for the OVF at the first floor. On the contrary, in winter, the performance of the OVFs is just the opposite: the OVF at the second floor has a lower heat flux than the one at the first floor, being the difference now between the two floors of about 3% as is shown in Table 2. On the other hand, in spring and autumn, the differences between the heat flux for the OVF on the first and second floors are a 3.35% lower in spring and a 1.26% higher in autumn. These results can be interpreted as the fact previously reported in the literature of an increase in air temperature in the ventilated channel with increasing height, which is beneficial in reducing the total heat flux in the cold weather period but results in an increase in heat flux in the hot weather season.

Regarding the total heat flux for the whole year, the value of this flux for the OVF at the first floor height is very close to the flux for the OVF at the second floor height, specifically, this difference is only of 0.43 kWh/m^2 that represents a 0.81% of difference between both fluxes, which is an indicator of the balancing effect on the annual heat flux that produces the opposite behavior of the heat exchange through the OVF in the cold and warm seasons produced by the OVF height.

On the other hand, the YHF obtained for the OVF at the height of the first floor height is equal to 41.43 kWh/m^2 which represents a reduction of 0.46 kWh/m^2 with respect to the YHF value obtained for the original OVF. This reduction in YHF, although small, is in agreement with previous results in the literature indicating that an increase in the height of the OVF improves its energy performance.

Finally, it can be concluded that, as can be seen in Fig. 17 and Table 2, for the two floors analyzed, the OVF is able to reduce the heat flux along the entire façade when compared to the reference case and, thus, to provide energy savings for the entire year.

4.7. OVF optimum design

Finally, after obtaining for each design parameter the value that provides the lowest YHF, the yearly heat flux that results for the OVF configuration resulting from choosing the aforementioned optimal design values is calculated.

This configuration is presented in Table 3, as well as the results of the resulting yearly heat flux for such configuration.

As can be seen in Table 3, the configuration for the OVF obtained using the optimum values of the design parameters achieves a reduction in the yearly heat flux greater than 32%.

However, in view of the discussion of the previous results, it can be expected that the use of an outer lamina material that provides a reduction in outer lamina diffusivity in excess of 30%, an increase in the insulation layer above 0.1 m, or an increase in the height of the OVF, are factors that can improve the result provided by the OVF with

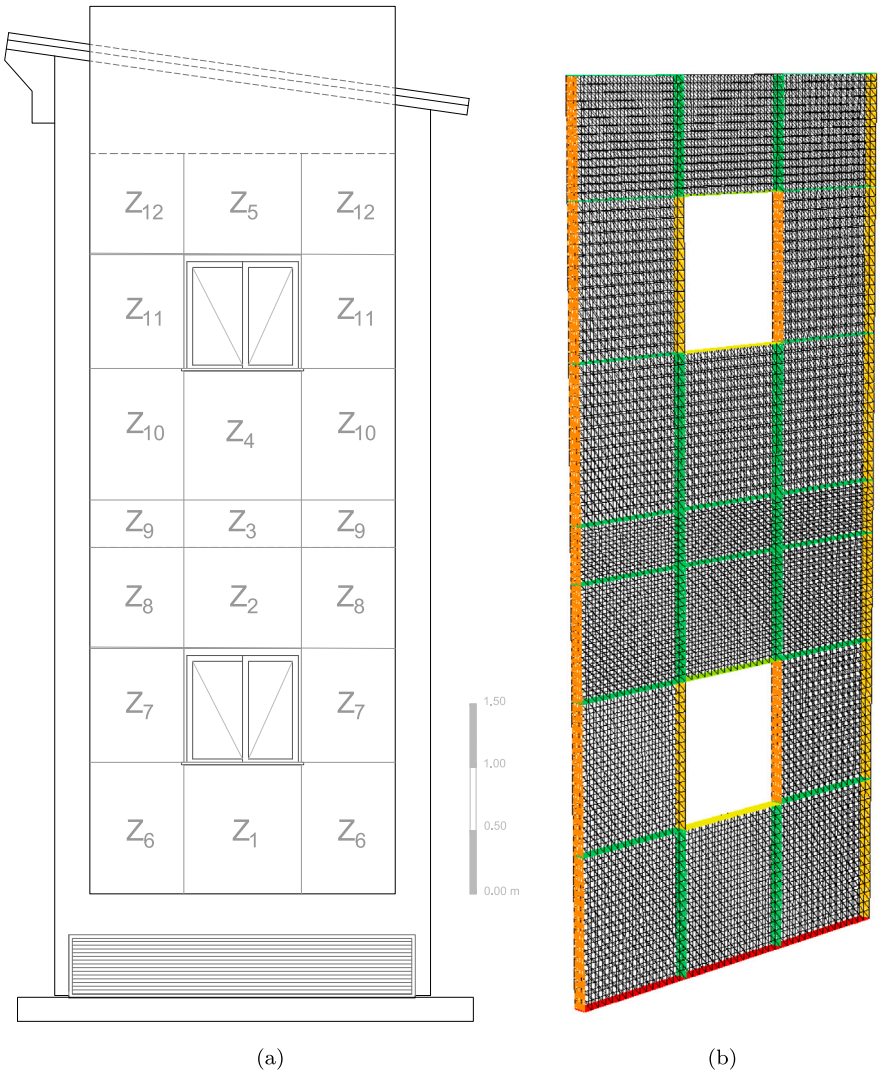

Fig. 13. Ventilated façade with two floors: (a) sketch; (b) 3D mesh of the ventilated chamber.

Table 2
Heat flux for the different OVF heights.

	Winter	Spring	Summer	Autumn	Whole year
First floor OVF: heat flux [kWh/m^2]	12.99	5.94	15.01	7.53	41.43
Second floor OVF: heat flux [kWh/m^2]	12.64	6.15	15.67	7.40	41.86
Reference case: heat flux [kWh/m^2]	13.39	7.45	23.86	8.29	53.01
Heat flux difference: first minus second floor [%]:	2.69	−4.23	−4.39	1.72	−1.03

Table 3
OVF configuration with optimum design values and resulting yearly heat flux.

Grill	Ventilated channel thickness	Solar Absorptivity	Thermal diffusivity	Insulation thickness	Yearly thermal flux [kWh/m^2]	Heat flux saving [%]
Open	0.15 m	0.4	−30%	0.1 m	35.67	32.71

the configuration presented in Table 3, although as stated above, it is possible that such changes would entail an increase in costs that may not be offset by savings in energy costs, a matter that would need to be elucidated by an appropriate economic analysis.

Finally, it should be noted that the annual heat flux through the OVF was calculated for OVF configurations with small changes, around 10%, from the values shown in Table 3 without finding a decrease of the YHF values, except for the case of the increase of the insulation thickness in which a small reduction, around 2%, of the YHF was found, although for the reasons stated in the previous paragraph and in Section 4.5, the implementation of insulation thickness values higher than 0.1 m seems inadvisable in the geographical and climatic framework of Southern Europe.

5. Conclusions

A well-validated three-dimensional CFD model has been used to analyze the influence of changes in the physical and geometric design parameters of an opaque ventilated façade with window openings in order to optimize its thermal behavior during a typical climatic year in the Mediterranean area.

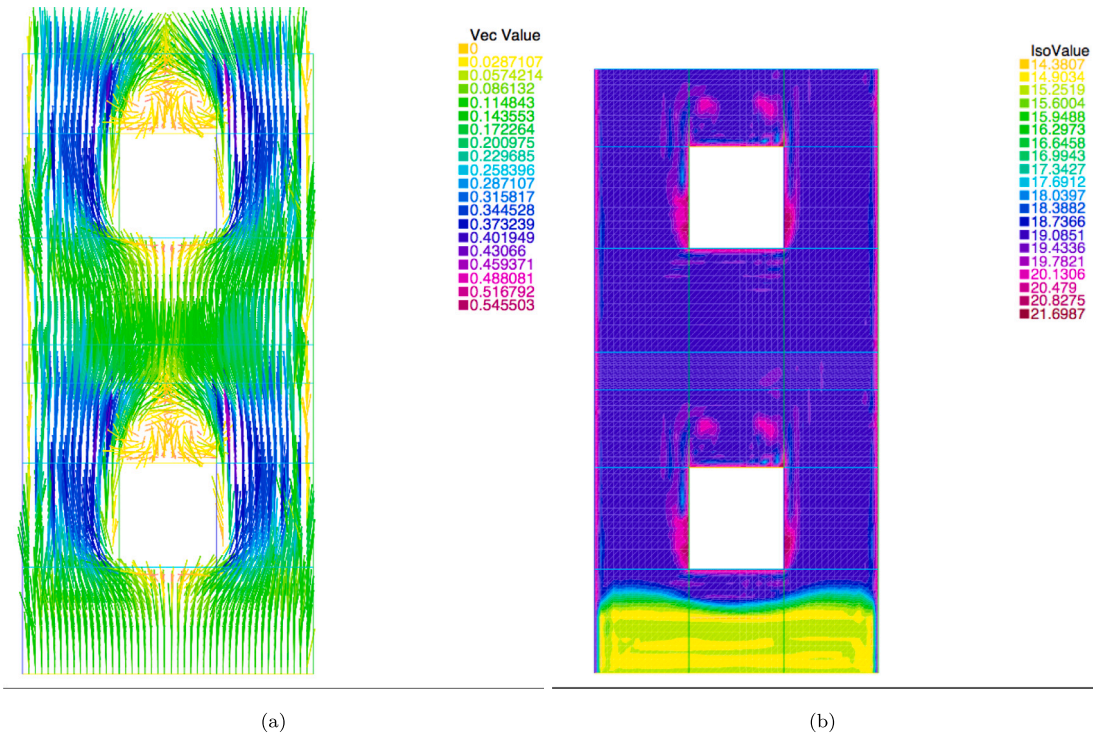

Fig. 14. Air in the ventilated chamber at noon, typical winter day: (a) velocity field; (b) temperatures. Velocity magnitude (Vec Value) and temperature isovalues (IsoValue) are shown in (a) and (b), respectively.

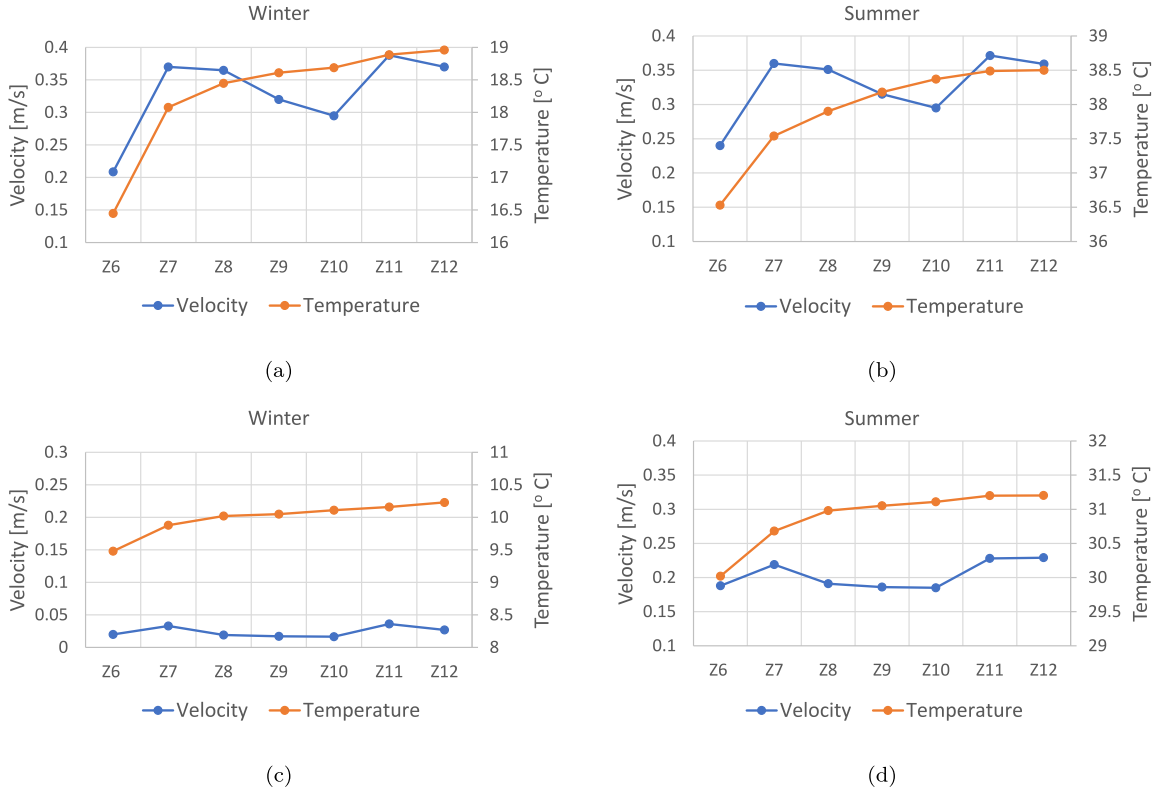

Fig. 15. Velocity and temperature of air in the middle section of the ventilated chamber as a function of the channel height computed at: (a) noon on a typical winter day; (b) noon on a typical summer day; (c) 18 h on a typical winter day; (d) 20 h on a typical summer day.

Variations in the yearly heat flux through the ventilated façade due to changes in the parameters studied have been computed. From the analysis performed, it has been possible to observe significant differences in the heat flux as a result of these changes.

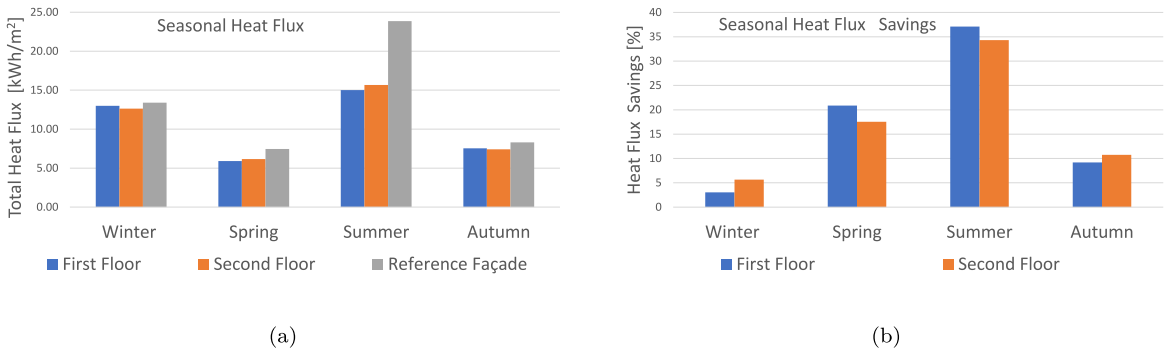

Fig. 16. Height of the ventilated façade: (a) seasonal thermal fluxes; (b) seasonal flux savings.

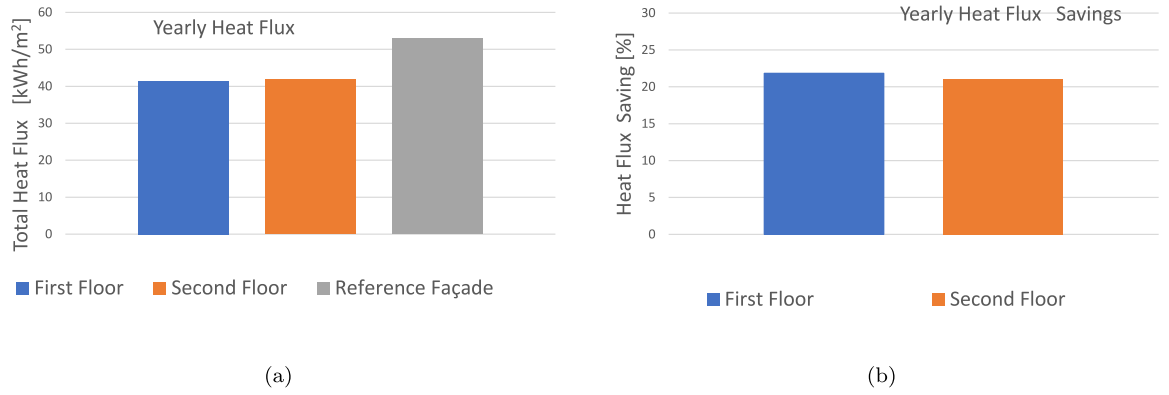

Fig. 17. Height of the ventilated façade: (a) yearly heat flux ; (b) yearly heat flux savings.

The yearly heat flux through for each facade configuration analyzed was compared to an unventilated reference façade typically used in social housing built in the middle of the last century in southern Europe, exhibiting good results in terms of reduction of heat flux in almost all cases. From the analysis carried out, it has been concluded that all the parameters analyzed have an influence on the energy performance of the OVF although this influence is sometimes more evident from a seasonal point of view than when considering the whole year because of the compensating effects that some parameters have on the heat flux in the different seasons.

The analysis of the results obtained from the research carried out allows us to reach the following conclusions, conclusions which, in turn, constitute guidelines for the efficient use of ventilated facades with windows for building retrofitting:

- The yearly heat flux through the OVF is lower when the opening grills are open than when they are closed. For open grills, the decrease in annual heat flux is 20.96% compared to the energy obsolete reference façade, while for closed grills reduction of YHF is by 15.17%. In the case where it is possible to establish a protocol of grill open in spring and summer and closed in winter and autumn, the reduction reaches the 26.09%.
- The increase in the thickness of the ventilated channel of the OVF for values below 0.1 m causes a significant decrease in the annual heat flux through the OVF. For values between 0.1 and 0.15 m the annual heat flux tends to increase slightly following a horizontal pattern. Once this value of 0.15 m is exceeded, the annual flux tends to increase almost linearly. Thus, it can be concluded that the minimum value of YHF and the maximum value of heat flux savings are found for a thickness of the ventilated chamber equal to 0.1 m.
- The heat flux through the OVF is strongly influenced by the solar absorptivity of the exterior surface of the outer layer; this heat flux has a convex behavior reaching its minimum for a value of the solar absorptivity equal to 0.4, and a maximum of the heat flux saving equal to a 21.42% for this value of the solar absorptivity.
- The thermal diffusivity of the OVF outer sheet has a relevant role in the heat flux performance. From the results obtained, it can be concluded that the lower the diffusivity of the outer layer, the lower the heat flux. So, the material that makes up this outer layer should be chosen with a diffusivity as low as possible.
- The assessment of the annual heat flux through the ventilated façade by varying the insulation thickness shows that the increase of this last produces a continuous decrease of the YHF that is very marked for values of thickness less than 0.06 m and tends to stabilize with a very lower decrease of the YHF for values between 0.12 and 0.2 m. Thus, from the results obtained it is suggested that a value for the insulation layer thickness between 0.6 and 0.1 m is the one that provides the more reasonable balance between cost of materials and energy cost savings.
- The height of the ventilated façade affects the yearly heat flux. Thus, increasing the height of the ventilated façade to two stories produces a slight decrease in the heat flux on the first floor compared to the single-story case, a decrease that, although somewhat smaller, is also observed on the second floor.
- The configuration for the OVP obtained using the optimum values of the design parameters achieves a reduction in the yearly heat flux greater than 32%.

The results summarized in this paper are novel as long as the parametric energy optimization performed here is focused on an opaque ventilated façade with windows opening, not previously discussed in the literature. Additionally, the study covers all seasons of the year, whereas most studies on ventilated facades focus on showing warm season results The findings presented here could be used in the preliminary stages of design and decision making for the energy retrofitting of buildings with energy obsolete façades, as well as for new construction.

Table 4
Customizable south wall thermophysical properties (Cell C3).

Layer	Description	Thickness (m)	Density (kg/m^3)	Specific heat (J/kg K)	Conductivity (W/m K)
1 (Out.)	Cement rendering	0.015	1300	1000	0.670
2	Perforated brick	0.115	780	1000	0.350
3	Cement rendering	0.010	1300	1000	0.670
4	Air chamber	0.050	1.184	1007	0.025
5	Hollow brick	0.040	770	1000	0.320
6 (Int.)	Gypsum plaster	0.015	1000	1000	0.570

Table 5
OVF thermophysical properties (Cell C1).

Layer	Description	Thickness (m)	Density (kg/m^3)	Specific heat (J/kg K)	Conductivity (W/m K)
1 (Out.)	Cement rendering	0.0050	1300	1000	0.670
2	Reinforced cement board	0.0125	1150	1000	0.350
3	Waterproof coat	0.0050	260	1000	0.050
4	Air gap	0.1000	1.205	1007	0.025
5	Wool rock panel	0.0500	100	840	0.046
6–11 (Int.)	Same as layers 1 to 6 of cell C3 south wall (Table 4).				

Table 6
Thermophysical properties of east and west walls, floor and roof.

Layer	Description	Thickness (m)	Density (kg /m^3)	Specific Heat (J/kg K)	Conductivity (W/m K)
1 (Out.)	Sandwich panel	0.200	40	1884.15	0.017
2	Wool rock panel	0.160	100	840	0.046
3 (Int.)	Sandwich panel	0.100	40	1884.15	0.017

CRediT authorship contribution statement

Carlos-Antonio Domínguez-Torres: Conceptualization, Methodology, Software, Validation, Formal analysis, Investigation, Data curation, Writing – original draft, Writing – review & editing, Visualization. **Rafael Suárez:** Conceptualization, Methodology, Validation, Formal analysis, Investigation, Writing – review & editing, Project administration, Funding acquisition. **Angel Luis León-Rodríguez:** Conceptualization, Methodology, Validation, Formal analysis, Investigation, Writing – review & editing, Project administration, Funding acquisition. **Antonio Domínguez-Delgado:** Conceptualization, Methodology, Validation, Formal analysis, Investigation, Writing – review & editing.

Declaration of competing interest

The authors declare that they have no known competing financial interests or personal relationships that could have appeared to influence the work reported in this paper.

Acknowledgments

This research was funded by the Ministry of Economy and Competitiveness of the Spanish Government and the European Regional Development Fund through the research and development project "Parametric Optimization of Double Skin Facades in the Mediterranean Climate to Improve Energy Efficiency Under Climate Change Scenarios" (ref BIA2017-86383-R). All authors have read and approved the final manuscript.

Appendix A. Test cells envelope characterization

The values shown in the tables in this section are those established in the Spanish Technical Building Code [52] and manufacturers' information.

Table 7
ASHRAE Guideline-14, FEMP and IPMVP Criteria for Validation of Models.

	Model Validation Criteria for Hourly Data		
Index	AHSRAE	FEMP	IPMVP
$NMBE(\%)$	$\in [-10, 10]$	$\in [-10, 10]$	$\in [-5, 5]$
$CV(RMSE)(\%)$	<30	<30	<20
	Model recommended value		
Index	AHSRAE	FEMP	IPMVP
r^2	>0.75	>0.75	–

Appendix B. Validation index summary

The aforementioned agencies, ASHRAE, FEMP and IPMVP, state that a model be considered validated when the results provided by the model meet the criteria shown in Table 7.

For the different time intervals and grill opening protocols involved in the validation process, the results obtained can be summarized as shown in Tables 8 and 9 where the minimum and maximum values of the statistical variables presented in Table 7 are shown for the computed variables. In Table 8 these values of the statistical validation variables are shown for the air temperature and velocity in the ventilated channel and the temperature of the different surfaces of the OVF while in Table 9 the values of the statistical indicators of Table 7 are shown for the heat transferred through the OVF.

As can be seen in these tables, the values of the statistical markers are inside the limits shown in Table 7 to consider validated a model. More details about the validation process can be found in [26].

Appendix C. Calculation of façades transmittance

The calculation of the transmittance U_{ref} of the reference façade is carried out in a standard way taking into account the values displayed in Table 4. Thus, to calculate U_{ref}, first the total thermal resistance of the reference façade is calculated as

$$R_{ref} = \sum_{i=1}^{6} R_i \tag{3}$$

Table 8
Minimum and maximum values of the statistical indicators for the velocity and temperature of air.

Index	Cavity air temperature		Cavity surfaces temperature		Cavity air velocity	
	Min	Max	Min	Max	Min	Max
			Grill open			
$NMBE$ (%)	−1.85	−8.66	−0.01	−1.40	−3.99	9.50
$CV(RMSE)$ (%)	6.11	15.12	2.12	2.87	11.71	23.39
r^2	0.7901	0.9101	0.9081	0.9716	0.7409	0.8090
			Grill closed			
$NMBE$ (%)	−1.39	−8.97	−0.06	−2.33	3.95	8.53
$CV(RMSE)$ (%)	5.94	13.97	1.84	3.53	11.09	21.09
r^2	0.9628	0.8961	0.9031	0.9634	0.7429	0.8322

Table 9
Values of the statistical markers for the heat transferred though the OVF.

Index	Grill open			Grill closed		
	Winter	Spring	Summer	Winter	Spring	Summer
$NMBE$ (%)	3.89	2.06	5.34	2.16	3.39	4.19
$CV(RMSE)$ (%)	12.79	10.21	16.33	9.80	10.08	13.05
r^2	0.8890	0.9133	0.8301	0.9021	0.9221	0.8499

where

$$R_i = \frac{e_i}{\lambda_i}, \quad i = 1, \ldots, 6$$

being e_i and λ_i the thickness and the conductivity of the ith layer of the reference façade for $i = 1, \ldots, 6$, except for the layer $i = 4$, the closed air gap, whose thermal resistance is directly taken from [53] that provides a value $R_4 = 0.18$ for unventilated vertical chambers of thickness $e = 5$ cm and horizontal heat flux.

Finally, the transmittance of the reference façade is computed as

$$U_{ref} = \frac{1}{R_{ref}} \tag{4}$$

Taking into consideration the values of Table 4, the value obtained for the reference façade transmittance is:

$$U_{ref} = 1.43 \quad [\mathrm{W/m^2\ K}].$$

For the OVF only the transmittance U_{IW} of the inner wall is calculated. The inner wall of the OVF is the result of adding a 5 cm thick insulation layer to the outer face of the reference façade as is described in the OVF layout shown in Table 5

The procedure is the same as for the reference façade; thus, the total thermal resistance R_{IW} of the inner wall of the OVF is calculated taking into account the additional 5 cm insulation layer added to the reference facade and the values of Table 5. In this way, the obtained value of the transmittance of the inner wall of the OVF is

$$U_{IW} = 0.56 \quad [\mathrm{W/m^2\ K}].$$

In the previous literature, it is possible to find works in which the transmittance was calculated considering all the layers that make up the OVF. Thus, in [37] the transmittance of three types of ventilated facades was calculated neglecting the thermal resistance of the air layer and of all other layers between the air layer and the external environment, and including an external surface resistance corresponding to still air. However, in the present work, as described above, in the case of the OVF only the transmittance value of the internal wall is estimated, and this is for information purposes, since in the energy and thermodynamic calculations performed in the research the values used are those shown in Tables 4, 5 and 6, i.e., thermal conductivity, specific heat, density, and thickness of each layer.

Table 10
Description of the sensors installed at the weather station on the Cell 3 roof.

Measured variable	Type of sensor	Accuracy	Rank
External air temperature	Thermometer	±0.75 °C	−40, 80 °C
Wind speed	Anemometer	±0.5%	0 to 50 m/s
Wind direction	Vane	±2.5%	0 to 360°
Relative humidity	Hygrometer	±3%	0 to 100%
Global irradiance	Pyranometer	±1.5%	0 to 2000 W/m^2
Diffuse irradiance	Pyranometer	±1.5%	0 to 2000 W/m^2

Appendix D. Monitoring equipment

For the experimental measurements used for calibration, the test cells have been equipped with a wide range of instrumentation. Four internal air temperature sensors and eight thermocouples are installed within each cell to monitor both air and surface temperatures, respectively. Indoor air temperature sensors are protected from solar radiation and installed in different positions and heights (1.5 m and 2.5 m).

Concerning the OVF, velocity and temperature sensors were placed along the centerline of the air cavity to measure air temperatures and velocities inside the OFV in a central position between the internal surface of the outer slab and the external surface of the internal wall at different heights and in five different positions. The temperatures of the outer slab and inner wall surfaces facing the ventilated chamber were recorded at heights identical to those of the air in the chamber. Fig. 18 shows a diagram depicting the placement of sensors in the OFV and the location of the sensors in the test cells is shown in Fig. 19.

The surface temperature sensors used are thermocouples of type K with an accuracy of ±1 °C and an operating range from −10 to 105 °C. The air temperature sensors have an accuracy of ±0.5 °C for a range from +10 to 30 °C and an accuracy of ±1 °C for a range from −5 to 10 °C and from 30 to 55 °C. All the temperature sensors were shielded against long-wave and short-wave radiation. The velocity sensors have an accuracy of ±0.05 m/s for a velocity range of 0.15 to 2 m/s.

Weather variables were measured from a weather station located on the roof of the Cell 3. A set of 5 pyranometers with north, east, south, west and horizontal orientations was used to measure solar radiation. Wind speed and direction were measured using an anemometer and a vane. The ambient temperature was measured using two shielded thermocouples. In Table 10 the characteristics of the weather sensors are shown.

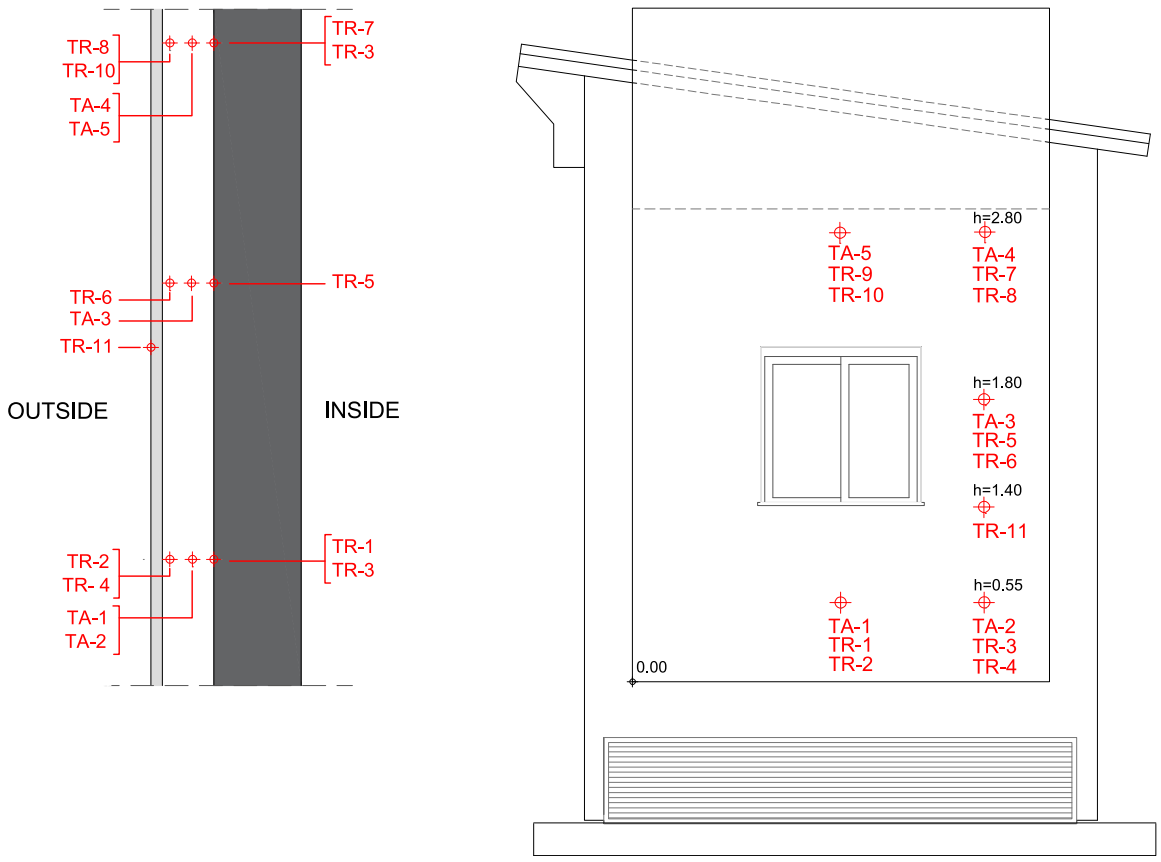

Fig. 18. Position of the monitoring sensors in the OVF.

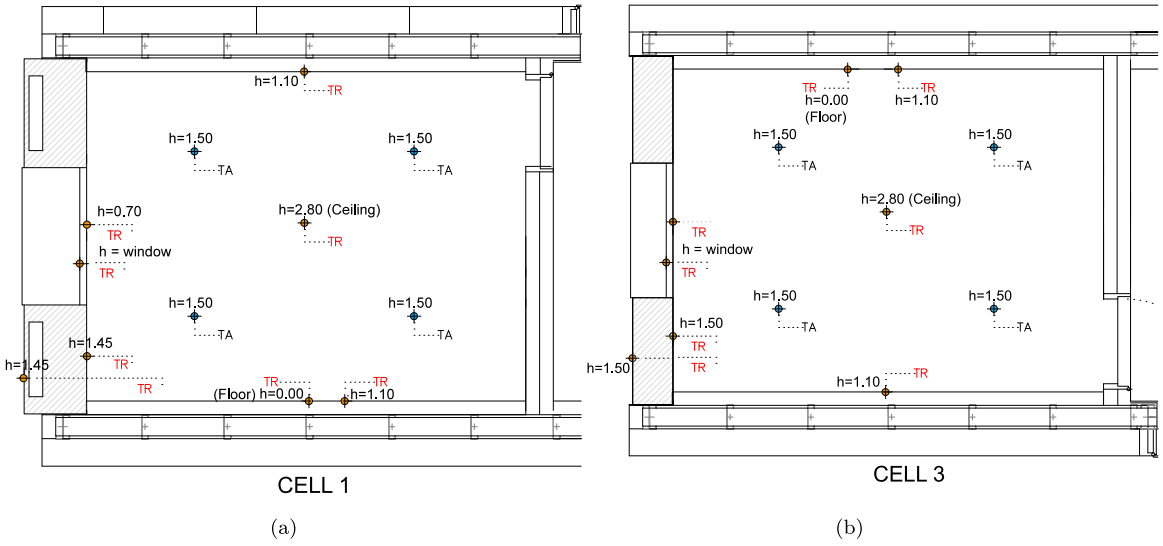

Fig. 19. Location of the sensors in: (a) Test cell 1; (b) Test cell 3. (TA air temperature sensors, TR surface temperature sensors; h indicates the height in meters).

References

[1] International Energy Agency, World energy outlook IEA, 2000.

[2] European Commission, DG energy; a policy framework for climate and energy in the period from 2020 to 2030, 2014, /* COM/2014/015 final */. Available online: HYPERLINK, https://op.europa.eu/en/publication-detail/-/publication/4ef2fc24-67d0-45c2-a6d1-c677574e6d26/language-en, https://eur-lex.europa.eu/legal-content/EN/TXT/.

[3] F. Kurtz, M. Monzón, B. López-Mesa, Energy and acoustics related obsolescence of social housing of Spain's post-war in less favoured urban areas: the case of Zaragoza, Inf. Constru. 67 (2015) m021, http://dx.doi.org/10.3989/ic.14.062.

[4] M. Gangolells, M. Casals, N. Forcada, M. MacArulla, E. Cuerva, Energy mapping of existing building stock in Spain, J. Clean Prod. 112 (2016) 3895–3904, http://dx.doi.org/10.1016/j.jclepro.2015.05.105.

[5] G. Semprini, R. Gulli, A. Ferrante, Deep regeneration vs shallow renovation to achieve nearly zero energy in existing buildings: energy saving and economic impact of design solutions in the housing stock of bologna, Energy Build 156 (2017) 327–342, http://dx.doi.org/10.1016/j.enbuild.2017.09.044.

[6] European Parliament, Directive 2002/91/ec of the european parliament and of the council of 16 december 2002 on the energy performance of buildings, Off. J. Eur. Union (2002) 65–71, http://dx.doi.org/10.1039/ap9842100196.

[7] C.A. Balocco, A simple model to study ventilated facades energy performance, Energy Build. 34 (2002) 469–475, http://dx.doi.org/10.1016/S0378-7788(01)

00130-X.
[8] M. Ciampi, F. Leccese, G. Tuoni, Ventilated facades energy performance in summer cooling of buildings, Sol. Energy. 75 (2003) 491–502.
[9] F. Patania, A. Gagliano, F. Nocera, A. Ferlito, A. Galesi, Thermofluid dynamic analysis of ventilated façades, Energy Build. 42 (2010) 1148–1155.
[10] A. Gagliano, F. Patania, A. Ferlito, F. Nocera, A. Galesi, Computational fluid dynamic simulations of natural convection in ventilated facades, evaporation, condensation and heat transfer, in: IntechOpen Book Series, 2011, http://dx.doi.org/10.5772/19817.
[11] C. Sanjuan, M.J. Suárez, M. González, J. Pistono, E. Blanco, Energy performance of anopen-joint ventilated façade compared with a conventional sealed cavity façade, Sol. Energy 85 (2011) 1851–1863, http://dx.doi.org/10.1016/j.solener.2011.04.028.
[12] A. Gagliano, F. Nocera, S. Aneli, Thermodynamic analysis of ventilated façades under different wind conditions in summer period, Energy Build. 122 (2016) 131–139, http://dx.doi.org/10.1016/j.enbuild.2016.04.035.
[13] M. Ibanez-Puy, M. Vidaurre-Arbizu, J.A. Sacristán-Fernández, C. Martín-Gómez, Opaque ventilated façades: Thermal and energy performance review, Renew. Sustain. Energy Rev. 79 (2017) 180–191.
[14] A. De Gracia, A. Castell, L. Navarro, E. Oro, L.F. Cabeza, Numerical modelling of ventilated façades: A review, Renew. Sustain. Energy Rev. 22 (2013) 539–549.
[15] S. Fantucci, V. Serra, C. Carbonaro, An experimental sensitivity analysis on the summer thermal performance of an opaque ventilated façade, Energy Build. 225 (2020) 110354, http://dx.doi.org/10.1016/j.enbuild.2020.110354.
[16] A. Gagliano, F. Nocera, S. Aneli, Thermodynamic analysis of ventilated façades under different wind conditions in summer period, Energy Build. 122 (2016) 131–139, http://dx.doi.org/10.1016/j.enbuild.2016.04.035.
[17] M.J. Suárez, C. Sanjuan, A.J. Gutiérrez, J. Pistono, E. Blanco, Energy evaluation of an horizontal open joint ventilated façade, Appl. Therm. Eng. 37 (2012) 302–313.
[18] C. Marinosci, G. Semprini, G.L. Morini, Experimental analysis of the summer thermal performances of a naturally ventilated rainscreen façade building, Energy Build 72 (2014) 280–287, http://dx.doi.org/10.1016/j.enbuild.2013.12.044.
[19] N. Mingotti, T. Chenvidyakarn, A.W. Woods, The fluid mechanics of the natural ventilation of a narrow-cavity double-skin facade, Build Environ. 46 (2011) 807–823, http://dx.doi.org/10.1016/j.buildenv.2010.09.015.
[20] Y. Tao, H. Zhang, L. Zhang, G. Zhang, J. Tu, L. Shi, Ventilation performance of a naturally ventilated double-skin façade in buildings, Renew. Energy 167 (2021) 184–198, http://dx.doi.org/10.1016/j.renene.2020.11.073.
[21] M. Labat, M. Woloszyn, G. Garnier, G. Rusaouen, J.J. Roux, Impact of direct solar irradiance on heat transfer behind an open-jointed ventilated cladding: experimental and numerical investigations, Sol. Energy 86 (2012) 2549–2560, http://dx.doi.org/10.1016/j.solener.2012.05.030.
[22] F. Stazi, A. Vegliò, C. Di Perna, Experimental assessment of a zinc-titanium ventilated façade in a mediterranean climate, Energy Build. 69 (2014) 525–534, http://dx.doi.org/10.1016/j.enbuild.2013.11.043.
[23] R. Pacheco, J. Ordóñez, G. Martínez, Energy efficient design of building: a review, Renew. Sustain. Energy Rev. 16 (2012) 3559–3573.
[24] J. Holman, Heat Transfer, McGraw-Hill Education, 2009.
[25] E. Giancola, C. Sanjuan, E. Blanco, M.R. Heras, Experimental assessment and modelling of the performance of an open joint ventilated façade during actual operating conditions in mediterranean climate, Energy Build 54 (2012) 363–375, http://dx.doi.org/10.1016/j.enbuild.2012.07.035.
[26] C.A. Domínguez-Torres, A.L. León-Rodríguez, R. Suárez, A. Domínguez-Delgado, Empirical and numerical analysis of an opaque ventilated facade with windows openings under mediterranean climate conditions, Mathematics 10 (2022) 163, http://dx.doi.org/10.3390/math10010163.
[27] F. Stazi, F. Tomassoni, A. Vegliò, C. Di Perna, Experimental evaluation of ventilated walls with an external clay cladding, Renewable Energy 36 (2011) 3373–3385.
[28] M.N. Sánchez, E. Giancola, M.J. Suáárez, E. Blanco, M.R. Heras, Experimental evaluation of the airflow behaviour in horizontal and vertical open joint ventilated facades using stereo-PIV, Renew. Energy 109 (2017) 613–623, http://dx.doi.org/10.1016/j.renene.2017.03.082.
[29] S. Fantucci, C. Marinosci, V. Serra, C. Carbonaro, Thermal performance assessment of an opaque ventilated façade in the summer period: calibration of a simulation model through in-field measurements, Energy Procedia 111 (2017) 619–628, http://dx.doi.org/10.1016/j.egypro.2017.03.224.
[30] Spanish royal decrete 2429/1979. Approving the basic building on thermal conditions in buildings NBE-CT-79, BOE Nro. 253 (1979) 24524–24550.
[31] P. Wouters, L. Vandaele, P. Voit, N. Fisch, The use of outdoor test cells for thermal and solar building research within the PASSYS project, Build. Environ. 28 (2) (1993) 107–113.
[32] P.A. Strachan, P.H. Baker, Outdoor testing, analysis and modelling of building components, Build. Environ. 43 (2) (2008) 127–128, http://dx.doi.org/10.1016/j.buildenv.2006.10.008.
[33] P. Seferis, P. Strachan, A. Dimoudi, A. Androutsopoulos, Investigation of the performance of a ventilated wall, Energy Build. 43 (2011) 2167–2178, http://dx.doi.org/10.1016/j.enbuild.2011.04.023.
[34] G. Diarce, A. Urresti, A. García-Romero, A. Delgado, A. Erkoreka, C. Escudero, Á. Campos-Celador, Ventilated active façades with PCM, Appl. Energy 109 (2013) 530–537, http://dx.doi.org/10.1016/j.apenergy.2013.01.032.
[35] A. Picallo-Perez, J.M. Sala-Lizarraga, Energy and exergy analysis of an experimental ventilated façade, Energy Build. 280 (2023) http://dx.doi.org/10.1016/j.enbuild.2022.112737.
[36] C. Alonso, I. Oteiza, J. García-Navarro, F. Martín-Consuegra, Energy consumption to cool and heat experimental modules for the energy refurbishment of façades. three case studies in madrid, Energy Build. 126 (2016) 252–262, http://dx.doi.org/10.1016/j.enbuild.2016.04.034.
[37] F. Stazi, G. Ulpiani, M. Pergolini, D. Magni, C.D. Perna, Experimental comparison between three types of opaque ventilated facades, Open Constru. Build. Technol. J. 12 (2018) 296–308, http://dx.doi.org/10.2174/1874836801812010296.
[38] M. Coussirat, A. Guardo, E. Jou, E. Egusquiza, E. Cuerva, P. Alavedra, Performance and influence of numerical sub-models on the CFD simulation of free and forced convection in double-glazed ventilated façades, Energy Build. 40 (2008) 1781–1789.
[39] C. Buratti, D. Palladino, E. Moretti, R.D. Palma, Development and optimization of a new ventilated brick wall: CFD analysis and experimental validation, Energy Build. 168 (2018) 284–297, http://dx.doi.org/10.1016/j.enbuild.2018.03.041.
[40] R. Li, A. Pitts, Y. Li, Buoyancy-driven natural ventilation of a roomwith large openings, Build Simul. (2007) 984–991.
[41] S. Auliac, A. Le Hyaric, J. Morice, F. Hecht, K. Ohtsuka, O. Pironneau, FreeFem++, third ed., 2017, pp. 31–32, Version 3.
[42] ASHRAE guideline 14-2014: Measurement of energy, demand, and water savings. ASHRAE: American society of heating, refrigerating and air conditioning engineers (atlanta, Georgia), 2014.
[43] U.S. department of energy office of scientific and technical information, 2002, https://www.nrel.gov/docs/fy02osti/31505.pdf.
[44] Federal Energy Management Program. Measurement and Verification Guidelines: Measurement and Verification for Federal Energy Projects Version 3.0. DOE (2008) US..
[45] K.A.R. Ismail, J.R. Henríquez, Two-dimensional model for the double glass naturally ventilated window, Int. J. Heat Mass Transfer 48 (2005) 461–475.
[46] ANSI/ASHRAE Standard 140-2001, American Society of Heating, Refrigerating and Air-Conditioning Engineers, Inc., 2001.
[47] A.R. Gentle, J.L.C. Aguilar, G.B. Smith, Optimized cool roofs: Integrating albedo and thermal emittance with R-value, Sol. Energy Mater. Sol. Cells 95 (12) (2011) 3207–3215, http://dx.doi.org/10.1016/j.solmat.2011.07.018.
[48] M. Rossi, V.M. Rocco, External walls design: The role of periodic thermal transmittance and internal areal heat capacity, Energy Build. 68 (2014) 732–740, http://dx.doi.org/10.1016/j.enbuild.2012.07.049.
[49] K. Saafi, N. Daouas, A life-cycle cost analysis for an optimum combination of cool coating and thermal insulation of residential building roofs in Tunisia, Energy 152 (2018) 925–938, http://dx.doi.org/10.1016/j.energy.2018.04.010.
[50] Reglamento de instalaciones térmicas en los edificios. Ministerio para la transición ecológica y el reto demográfico. Decreto 178/2021, de 23 de marzo, 2021, https://energia.gob.es/desarrollo/EficienciaEnergetica/RITE/Paginas/InstalacionesTermicas.aspx. (Last Accesed 20 November 2021).
[51] Agencia estatal de meteorología de españa, 2010, Guía resumida del clima en España (1981-2010).
[52] Código Técnico de la Edificación, 2009, Ministerio de Fomento del Gobierno de España. Madrid, Spain..
[53] DB-HE Ahorro de energía. Código Técnico de la Edificación, 2009, Ministerio de Fomento del Gobierno de España. Madrid, Spain. https://www.cgate.es/hit/Hit2016-2/DA-DB-HE-1-Calculodeparametroscaracteristicos.pdf.